

We are IntechOpen, the world's leading publisher of Open Access books Built by scientists, for scientists

6,900

Open access books available

186,000

International authors and editors

200M

Downloads

Our authors are among the

154

Countries delivered to

TOP 1%

most cited scientists

12.2%

Contributors from top 500 universities



WEB OF SCIENCE™

Selection of our books indexed in the Book Citation Index
in Web of Science™ Core Collection (BKCI)

Interested in publishing with us?
Contact book.department@intechopen.com

Numbers displayed above are based on latest data collected.
For more information visit www.intechopen.com



Heterogeneous Catalytic Process for Wastewater Treatment

Ting Zhang

Abstract

This chapter introduced heterogeneous catalysis and described diverse heterogeneous catalytic processes for wastewater treatment. The main advantages of heterogeneous catalysis were explained compared with homogeneous catalysis. The methods of synthesis and characterization of heterogeneous catalysts with some examples were then elaborated. The principle of heterogeneous catalytic treatment process of refractory wastewater was analyzed, and several different types of heterogeneous catalytic oxidation processes, technical progresses, and application examples were presented. The mechanisms of heterogeneous catalytic oxidation degradation of pollutants in wastewater were also discussed. According to the review, the heterogeneous catalytic oxidation technology was considered having a good application prospect, and the further research directions of heterogeneous catalysis were proposed.

Keywords: heterogeneous catalysis, synthesis, characterization, wastewater treatment, refractory wastewater, catalytic oxidation processes, mechanism

1. Introduction

Water pollution, especially organics pollution, has become a global environmental problem. The severity, nature, and harm to organisms and human beings of organic pollution are continually changing with the development of society and industry. In recent years, the pollution of refractory organics and their treatment have become a hot topic to researchers all over the world. Refractory organic pollutants, such as halogenated organics, surfactants, nitro compounds, heterocyclic compounds, phenolic compounds, and polycyclic aromatic hydrocarbon, among others, with high toxicity, are difficult to be degraded by microorganisms. Many of these pollutants have toxic effects on humans and organisms, such as carcinogenic, teratogenic, and mutagenic effects. The harmfulness of refractory organic compounds has posed a severe threat to human health and ecosystems. Therefore, how to control the pollution of refractory organics has always been an important research topic in the field of environmental protection.

Researchers have conducted in-depth studies on the treatment of wastewater containing refractory organics. Refractory organics can be removed by adsorption, advanced oxidation, and membrane separation, among others (**Figure 1**). Among these technologies, advanced oxidation processes (AOPs) have made remarkable progress and achievements in the treatment of wastewater containing refractory organics. AOPs, including photochemical oxidation, catalytic wet oxidation,

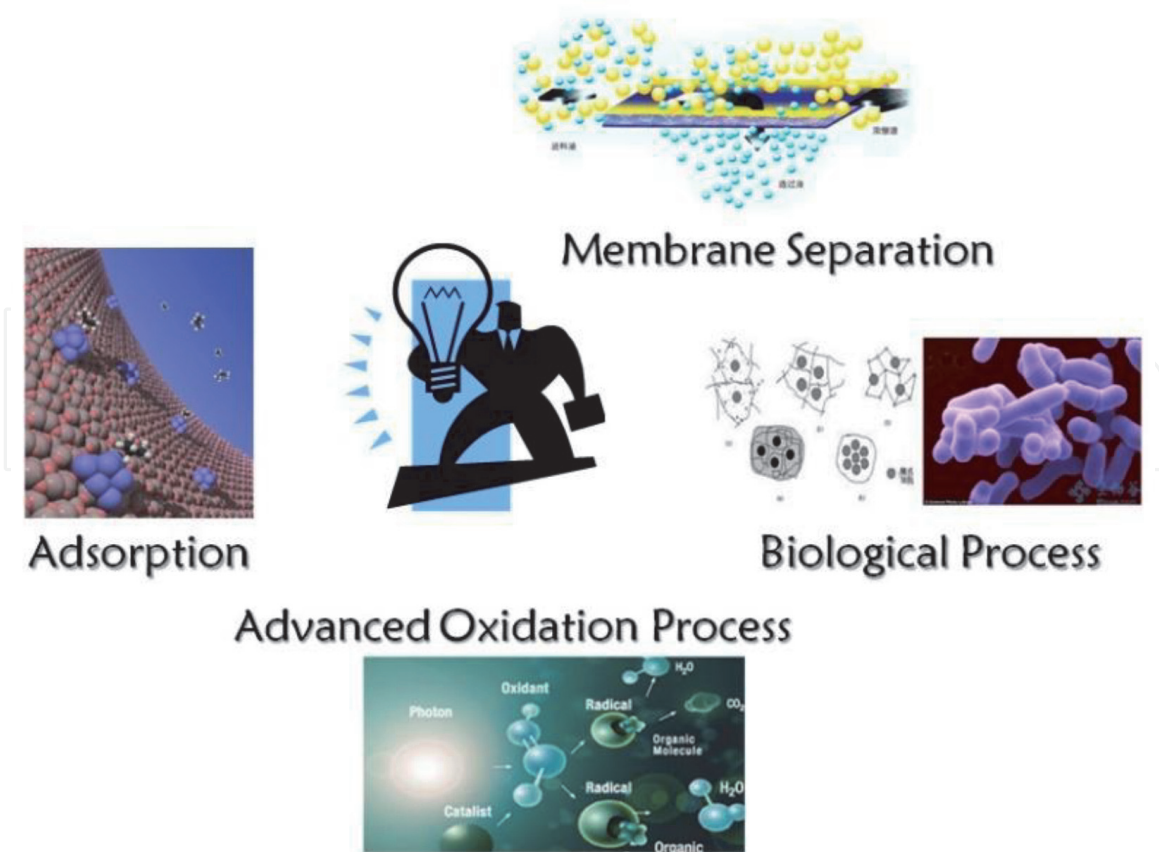


Figure 1.
Refractory organics removing methods.

sonochemical oxidation, electrochemical oxidation, and ozone oxidation, can decompose and transform toxic, harmful, and refractory macromolecular organics into nontoxic, harmless, and biodegradable small molecular organics. The final products of the oxidation are carbon dioxide, water, and inorganic ions, while no excess sludge is produced.

The catalysis term implies the process of increasing the rate of a chemical reaction by adding a catalyst, which is ultimately regenerated so that its amount remains unchanged. Catalysis is inhibited if the catalyst or the reactant is removed, or inhibitors alter the reaction. Inhibitors are materials that slow down the overall reaction by shortening the reaction chains, generally by reacting with one of the chemical components that maintain the chain and entering into a nonchain reaction. A wide variety of substances, such as phenols, sugars, and alcohols, have been found to act as inhibitors during the catalysis process.

The homogeneous catalysis occurs in a single phase, in which the catalyst is dispersed in an aqueous solution or gas mixture with the reactants. Conversely, heterogeneous catalysis occurs in more than one phase; for instance, the reactants are liquids, and the catalyst is solid [1].

AOPs' aim is to generate hydroxyl radicals ($\cdot\text{OH}$), which can oxidize most chemical species, especially hard-to-degrade organics. Hydroxyl radicals are nonselective when oxidizing organics, while their oxidation potential has been estimated as 2.8 and 1.9 V at pH 0 and 14, respectively [2].

The heterogeneous Fenton reaction has demonstrated better catalytic performance and environmentally friendly characteristics when compared with the homogeneous Fenton reaction. Although homogeneous catalysts are generally very efficient for the degradation of organic compounds, the catalysts of iron ions are dissolved in water, their separation and reuse are rather difficult at the end of treatment, and ferric ions are generated as by-products. The removal of iron ions

from the treated water needs a large number of chemicals and manpower, which will increase the cost of treatment. Another drawback is the tight range of pH in reactions of homogeneous Fenton systems. The pH of the solution in a Fenton system should be adjusted to around 3.0 before carrying out the wastewater treatment, and the reagents for acidification are very costly [3].

In this chapter, the preparation processes and characterization methods of heterogeneous catalysts, as well as treatment applications, are reviewed. This chapter aims to provide a basis for further studies on new heterogeneous catalysts for the treatment of refractory organics.

2. Heterogeneous catalysis

Many catalytic processes, in which the catalyst and the reactants are not present in the same phase, are heterogeneous catalytic reactions. They include reactions of gases (or liquids) at the surface of a solid catalyst. The surface is where reactions take place, so the catalysts are generally prepared to provide large surface areas per unit. Metals, metals coated onto supporting materials, metalloids, metallic films, and doped metals have all been used as heterogeneous catalysts.

With solid catalysts, at least two of the reactants are chemisorbed by the catalyst, and they will react at the surface of the catalyst, with which the products are formed as readily as possible. Then, the products are released from the catalyst surface, as can be seen in **Figure 2**.

Heterogeneous catalysts can be divided into two categories: unsupported catalysts (bulk catalyst) and supported catalysts. Unsupported catalysts include metal oxide catalysts, such as Al_2O_3 , SiO_2 , and B_2O_3 , and zeolite molecular sieve catalysts, such as ZSM-5, X, Y, and B types of zeolite. Supported catalysts often employ porous materials as supporters, and active components, metals or metal oxides, for example, are coated on the surface of the supporters to form the catalysts. Heterogeneous catalysts can accelerate many chemical processes, including CO oxidation, selective oxidation, water-gas shift, selective hydrogenation, electrocatalysis, photocatalysis, organic reactions, deNO_x , and reforming reactions, among others, as shown in **Figure 3**.

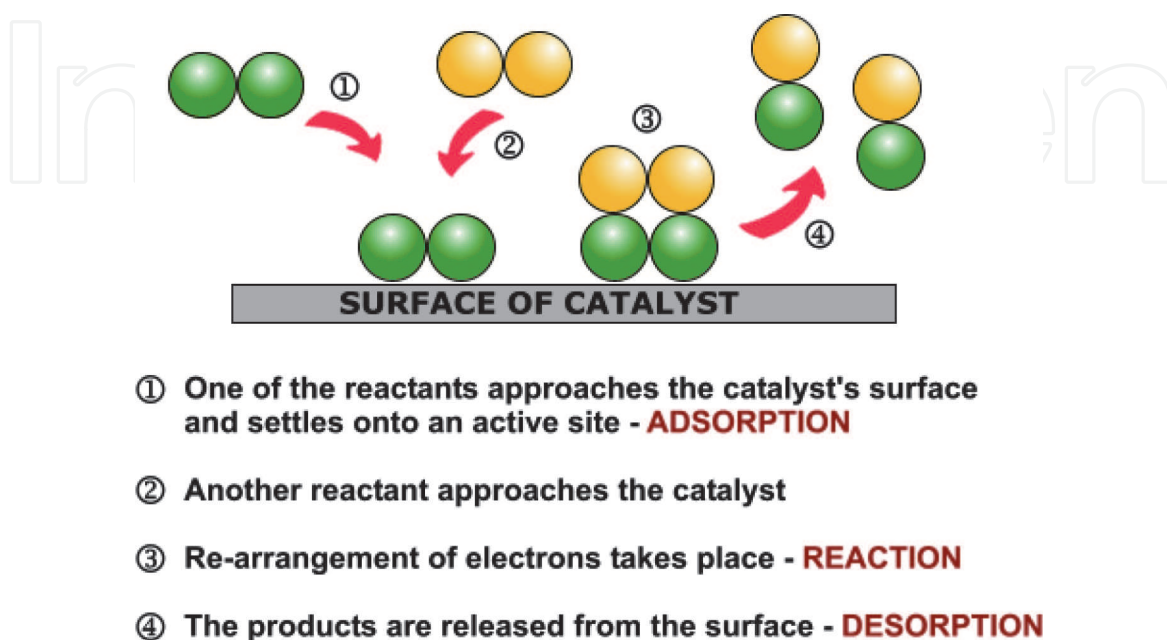


Figure 2.
Catalytic processes on a solid catalyst.

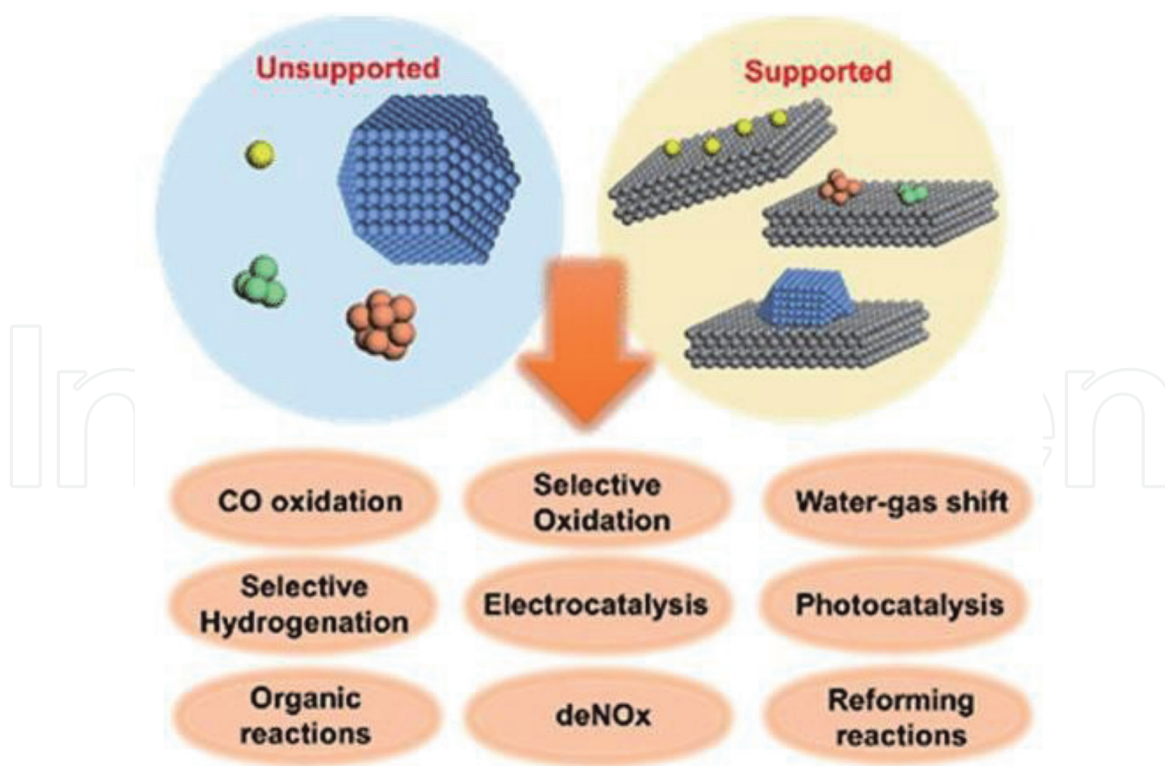


Figure 3.
Types of heterogeneous catalysts and their usages.

The heterogeneous catalytic process, as an efficient green method coping with organic wastewater, has attracted considerable attention in the last two decades. The highly reactive and nonselective hydroxyl radicals can oxidize and mineralize most organic compounds at near diffusion-limited rates, mainly unsaturated organic compounds.

3. Synthesis and characterization of heterogeneous catalysts

Catalysis is a surface phenomenon occurring on the surface or interface; in order for the catalyst to have more active sites, it is necessary to maximize its surface area, that is, to increase the porosity of solid catalysts. There are two ways to increase porosity. First, if the solid catalyst is composed of nonporous crystals, the catalyst should be prepared with the smallest grain size (i.e., to increase its external surface area). Second, if the solid catalyst is composed of grains with regular channels, the catalyst should be prepared by particles with regular channels (i.e., to increase its internal surface area). **Figure 4** shows the schematic of various catalyst development strategies, which aim to increase the number of active sites or increase the intrinsic activity of each active site.

To characterize heterogeneous catalysts, BET surface area, scanning electron microscope (SEM), transmission electron microscope (TEM), Fourier transform infrared spectroscopy (FT-IR), and X-ray diffraction (XRD) are commonly used characterizing methods.

The specific surface areas and pore volumes of the samples are often determined by physisorption of nitrogen at -196°C using a Micromeritics ASAP instrument. The specific surface area is calculated using the BET method and pore size distribution was obtained by using the BJH method.

A field-emission scanning electron microscope is utilized to determine the crystal morphology and chemical element composition. Measurements are made with

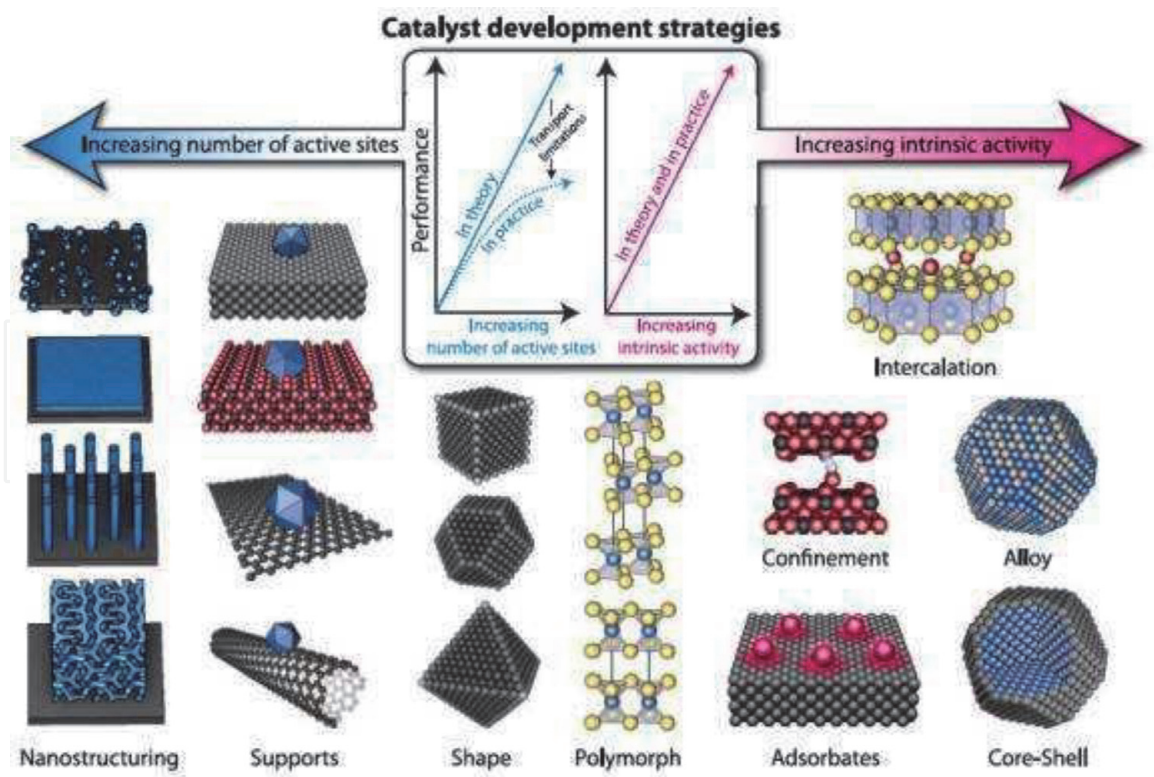


Figure 4.
Catalyst development strategies.

SEM using a digital imaging processing at room temperature and acceleration voltage of 20 kV. The samples are usually prepared as electrically conductive by sputter coating with a thin layer of gold under vacuum conditions to avoid charge accumulations of nonmetal catalysts, and all samples are dispersed in ethanol before tests.

A transmission electron microscopy is utilized to observe and analyze the micromorphology and microstructure. FT-IR spectroscopy is used to confirm the chemical structure, any changes in the compositional or functional group during the preparation of catalysts. Measurements are made on a FT-IR spectrometer after samples are mixed with 300 mg of spectroscopic grade KBr and ground in an agate mortaring in the range of $4000\text{--}400\text{ cm}^{-1}$ at room temperature.

To investigate the crystalline structure and stability of catalyst composites, powder X-ray diffraction patterns are recorded by X-ray diffractometer using $\text{Cu K}\alpha$ radiation ($\lambda = 0.1542\text{ nm}$) at a rate of $0.02^\circ/\text{s}$ in the range of $5\text{--}80^\circ$ with an operating voltage of 40 kV and electric current of 150 mA.

If the catalysts contain metals, XPS (X-ray photoelectron spectroscopy) of the samples are often tested. XPS was used to identify metal oxidation states of the composites.

3.1 Bulk catalysts

Bulk catalyst refers to the whole catalyst particle, its external surface, and internal components, where almost all of them are active substances. Some examples of bulk catalysts are silica-aluminum catalysts for catalytic cracking and ammonia synthesis, zinc-chromium oxide or copper-zinc-aluminum catalysts for hydrogen production, and iron molybdate catalysts for methanol oxidation [4–7]. The main chemical processes for the preparation of such catalysts are precipitation, gelation, and crystallization. **Figure 5** shows the synthesis processes of bulk catalysts.

$\text{LiFe}(\text{WO}_4)_2$ catalyst for decolorization of methylene blue is an example of bulk catalysts. $\text{LiFe}(\text{WO}_4)_2$ particles are prepared using solid-state reactions. The

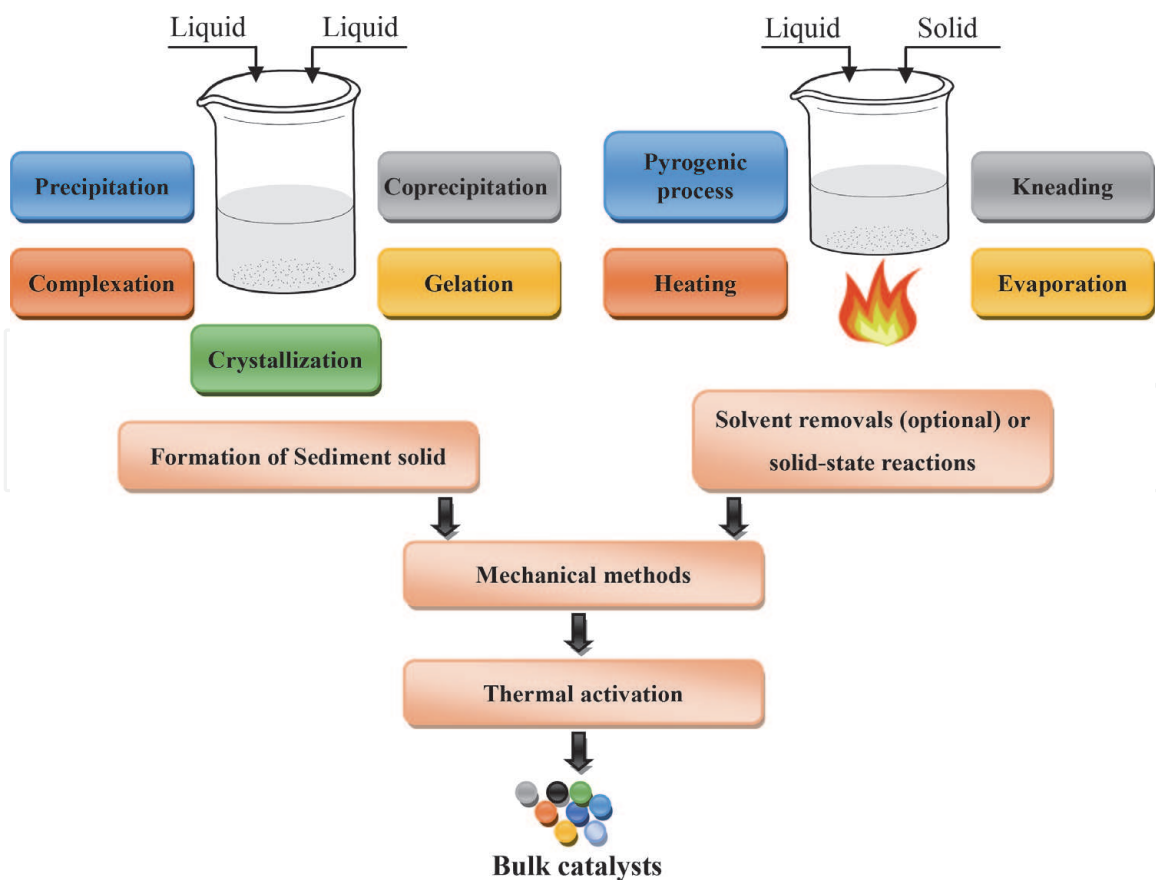


Figure 5. Synthesis process of bulk catalysts.

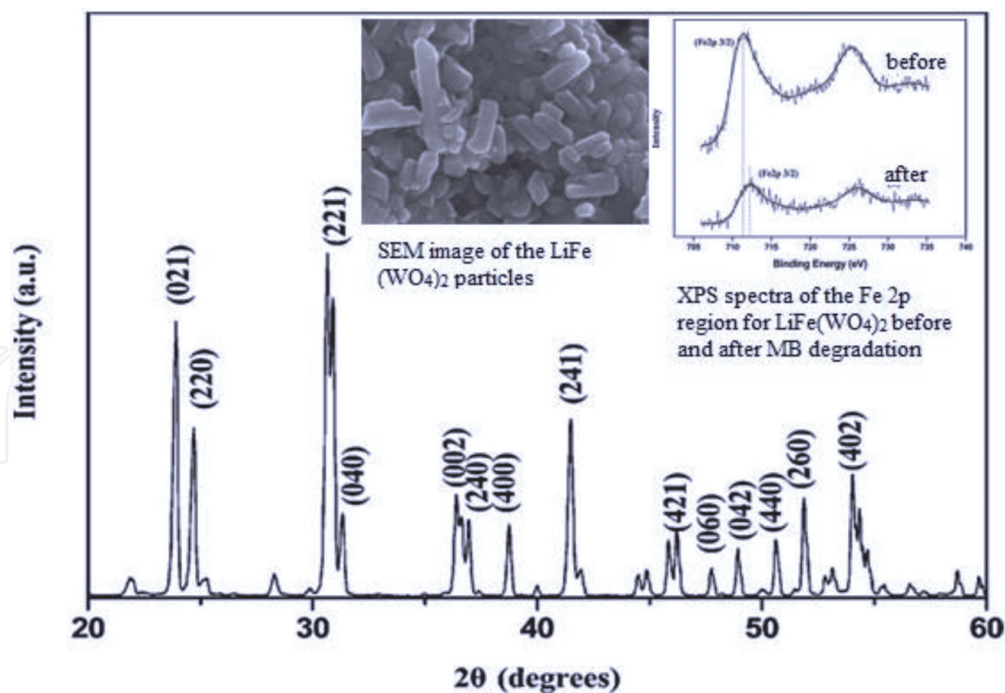


Figure 6. Characterizations of $\text{LiFe}(\text{WO}_4)_2$ catalyst [8].

powders, consisting of Li_2CO_3 , Fe_2O_3 , and WO_3 with a molar ratio of 1:1:4, are mixed uniformly in a glass mortar. Then, the mixture is mechanically milled with hydrous ethanol as a lubricating agent. Afterwards, the powders are dried to remove the ethanol. Finally, the powder is calcined and yields well-crystallized $\text{LiFe}(\text{WO}_4)_2$ [8].

The characterizations of $\text{LiFe}(\text{WO}_4)_2$ can be seen in **Figure 6** [8]. The XRD patterns of the $\text{LiFe}(\text{WO}_4)_2$ show that the peaks of the sample match well with the published standard data (PDF 01-072-0751), and $\text{LiFe}(\text{WO}_4)_2$ has a highly crystalline and single-phase structure, without any peaks of unreacted precursors. The morphological characteristic of the $\text{LiFe}(\text{WO}_4)_2$ particles shows that the $\text{LiFe}(\text{WO}_4)_2$ crystal was rod-like, that the average length of the samples varied over the range of 300–500 nm, and that the width of the sample was about 200 nm. XPS spectra show that the binding energy of 711.94 eV belongs to $\text{Fe}2p_{3/2}$. The binding energy value slightly decreased after 1 h reaction of MB decolorization due to the transformation of Fe(III) to Fe(II) after heterogeneous photo-Fenton reaction [8].

3.2 Supported catalysts

Supported catalysts are the most often used catalysts in wastewater treatment processes. They include the surface-loaded catalysts, core-shell catalysts, and thin-film catalysts.

3.2.1 The active catalytic components loaded onto the carrier surface

Surface-loaded catalysts mean active catalytic components loaded onto the carrier, which can be divided into two categories: one is concentrating the active components to the surface of porous solid carriers by means of dipping the carriers into the precursor contained ions or molecules and the other is that the predecessors or catalyst solid particles are adhered or deposited to the surface of the carrier, such as sol-gel method.

Carriers are inorganic porous materials, such as alumina, silicon oxide, activated carbon, zeolite, molecular sieve, and clays, among others. Commonly used catalyst carriers' structure data are shown in **Table 1**.

The most important supported catalysts are metal- or oxide-supported catalysts. Metal precursors are usually metal salts, such as nitrates, carbonates, sulfates, and chlorides. These salts are also the raw materials for preparing metal oxide supporters and bulk catalysts. When they dissolve in water, they will be dissociated into ions, and metal ions will further form hydrated ions. If the catalyst supporters are added to these metal salt solutions, the active components can be loaded onto the supporters by impregnation or sol-gel methods, thereby obtaining heterogeneous catalysts. **Figures 7** and **8** are typical processes of impregnation and sol-gel methods for heterogeneous catalyst synthesis.

Carriers		Specific surface area/(m^2/g)	Pore volume/(mL/g)
Oxide	Al_2O_3	200~500	0.3~0.9
	SiO_2	400~800	0.4~4.0
	$\text{SiO}_2\text{-Al}_2\text{O}_3$	400~600	0.5~0.9
	MgO	30~140	0.3
Carbon	Activated carbon	~1000	0.3~2.0
Clay	Bentonite	150~280	0.3~0.5
	Attapulgite	100~200	0.3~0.5

Table 1.
 Structure data of commonly used catalyst carriers.

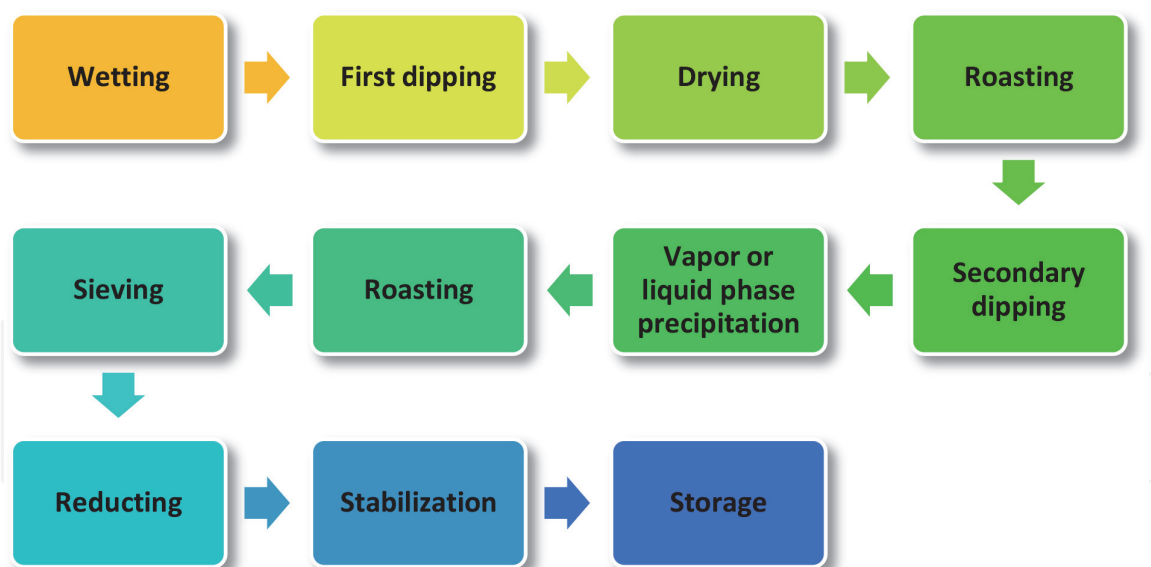


Figure 7.
Typical process of impregnation for heterogeneous catalyst synthesis.

3.2.1.1 Carbon-based catalysts

Carbon is often used as a catalyst supporter due to its large surface area and porous structure. There are many types of carbon: activated carbon, activated carbon fiber, mesoporous carbon, and multiwalled carbon nanotubes, among others. Here are some examples of carbon supporters for heterogeneous catalysts.

Ordered mesoporous carbon-supported iron catalysts (Fe/OMC) were prepared by the incipient wetness impregnation method [9]. OMC was prepared by triconstituent coassembly of resols, oligomer silicates from TEOS, and triblock copolymer F127 template, followed by carbonization and silica removal. The OMC was impregnated in an iron nitrate solution; then, the catalyst was dried, followed by calcination under N_2 flow.

Characterizations of Fe/OMC are shown in **Figure 9** [9]. From the XRD patterns, all of the samples show a broad peak at 23.5° corresponding to amorphous carbon. The crystallinity of iron oxides is improved with the increase of calcination temperature. TEM images showed a highly ordered array in the structure of OMC and Fe/OMC catalysts, which suggests the preservation of the long ordered arrangement of the channels after the iron deposition. The iron oxide particles are not clearly seen in the TEM image at a low calcination temperature of the samples, as the calcination temperature increases, the iron particles become more prominent and are revealed in the TEM images. The iron particles are well dispersed from the TEM pictures [9].

Fe_3O_4 /multiwalled carbon nanotubes (MWCNTs) were synthesized by in situ chemical oxidation coprecipitation. MWCNTs were pretreated by stirring in a flask, containing a mixture of sulfuric acid/nitric acid and refluxing in an ultrasound wave cleaner. The as-treated MWCNTs were suspended in deionized water and put into a $95^\circ C$ water bath. $FeSO_4 \cdot 7H_2O$ was added into the MWCNT suspended solution and NaOH and $NaNO_3$ solution was added dropwise, which is heated up to $95^\circ C$ into the heating MWCNT-metal solution with vigorous stirring as well as stable N_2 flow during the entire reaction period. After 2 hours, the Fe_3O_4 /MWCNT nanocomposites were formed [10].

Characterizations of Fe_3O_4 /MWCNTs are shown in **Figure 10** [10]. The TEM images show the octahedron Fe_3O_4 nanoparticles with diameters ranging from 40 to 100 nm growing on the MWCNTs surface regularly and most of the Fe_3O_4 nanoparticles were strung by MWCNTs. The room-temperature Raman spectra

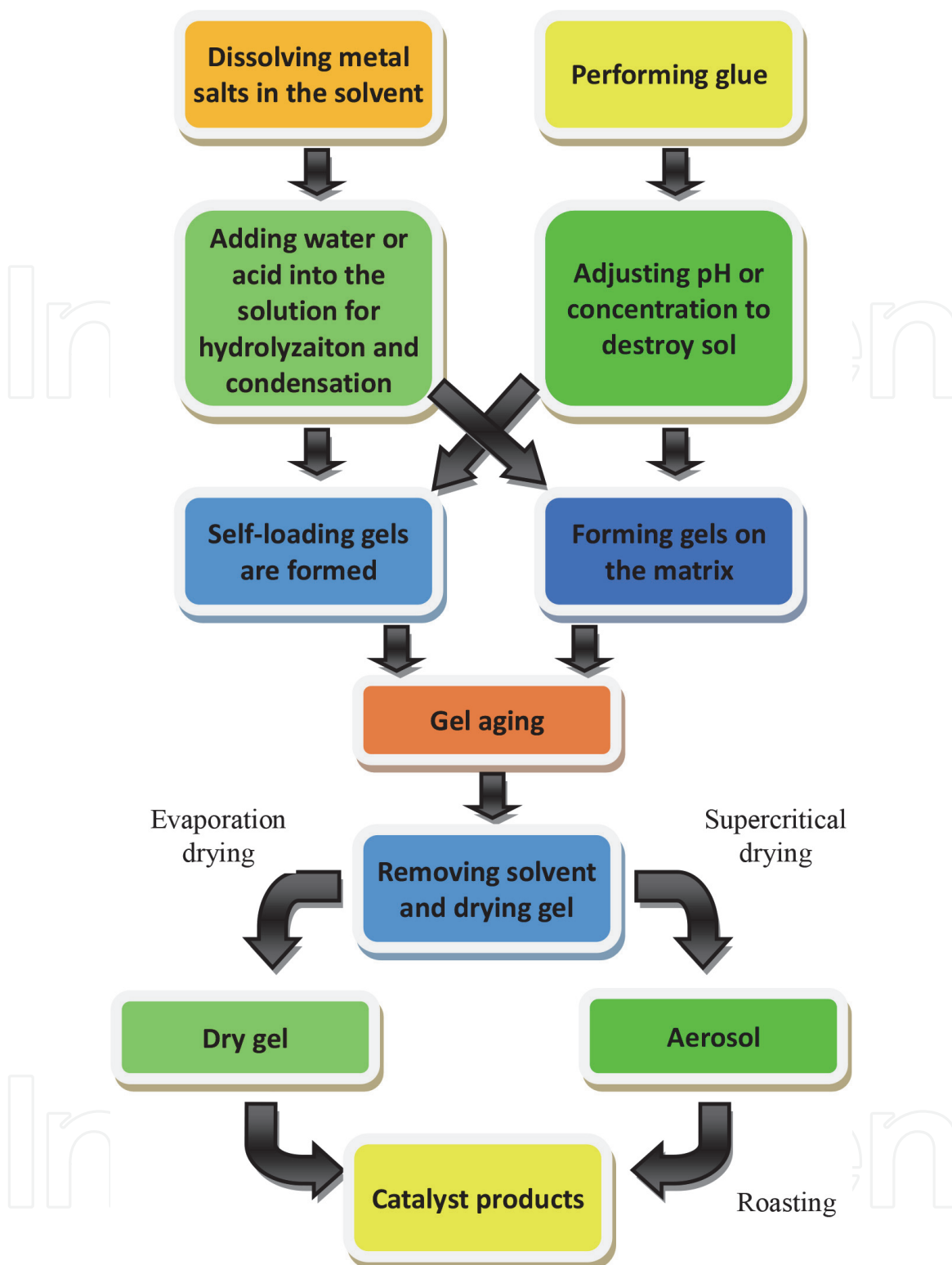


Figure 8.
Typical process of the sol-gel method for heterogeneous catalyst synthesis.

show a difference in the crystallinity of MWCNTs before and after the Fe_3O_4 loading process. Some extra peaks were observed at lower wave numbers corresponding to vibration modes of Fe-O bonds of Fe_3O_4 nanoparticles, and Fe-C bonds confirm the formation of Fe_3O_4 nanoparticles on the surface of MWNTs [10].

3.2.1.2 Oxide-based catalysts

Recently, metal-containing oxide-based (mesoporous silica, Al_2O_3 , and ZnO , among others) catalysts have attracted much attention because the oxide-based

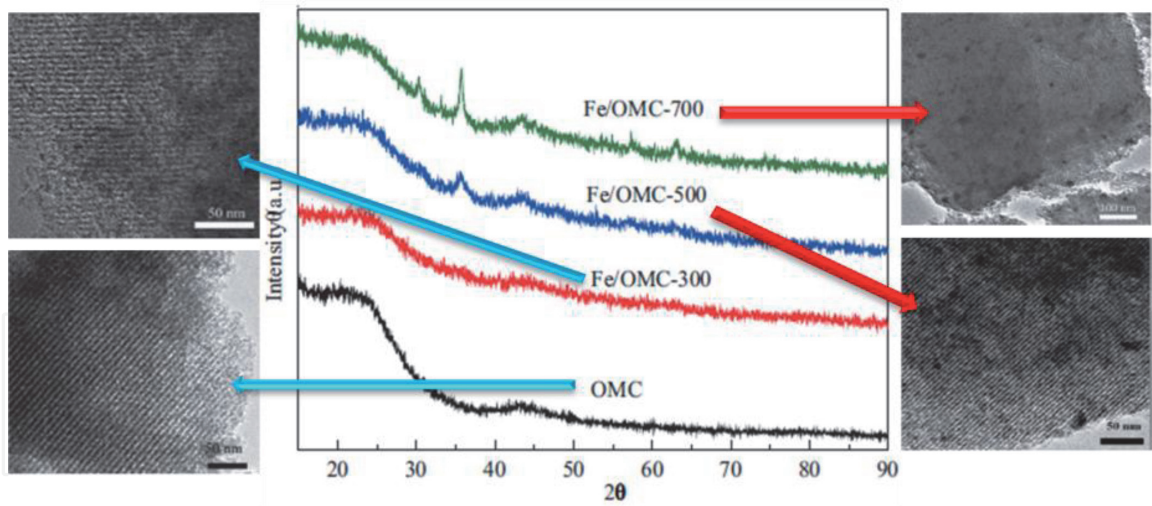


Figure 9.
Characterizations of Fe/OMC [9].

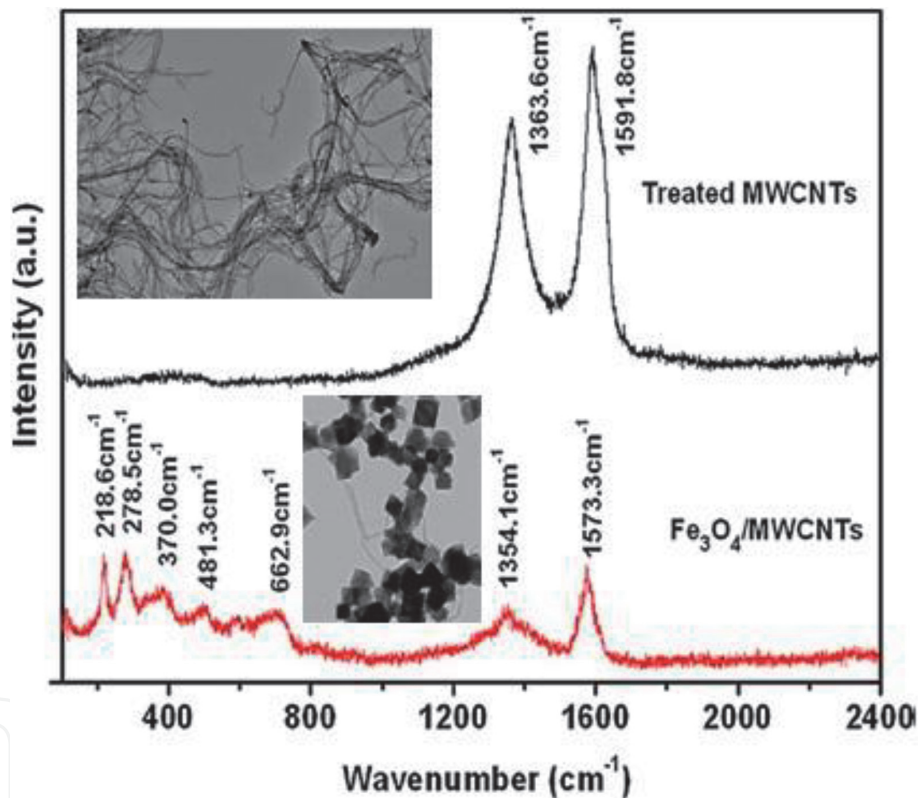


Figure 10.
Characterizations of $\text{Fe}_3\text{O}_4/\text{MWCNTs}$ [10].

materials have a high surface area, good thermal stability, and favorable hydrothermal stability. Numerous oxide-based composites were synthesized for degrading organic compounds such as methyl orange, acid orange, polyarylamide, and phenol [11–16].

The porous $\text{Fe}_2\text{O}_3\cdot\text{SiO}_2$ composite was prepared by a facile impregnation method [17]. Typically, silica powder was immersed in $\text{Fe}(\text{NO}_3)_3$ and the mixture was vigorously stirred for 24 h at room temperature; then, the sample was dried and calcined. The obtained powder was cooled to room temperature to get as-synthesized $\text{Fe}_2\text{O}_3\cdot\text{SiO}_2$ for catalytic experiments.

Characterizations of $\text{Fe}_2\text{O}_3\cdot\text{SiO}_2$ are shown in paper [17]; those figures present the FE-SEM and TEM images, EDS spectrum and EDS mapping image, XRD

patterns, N_2 adsorption/desorption isotherms, and FT-IR spectra of as-synthesized $Fe_2O_3 \cdot SiO_2$ and as-synthesized SiO_2 . As shown in SEM images, silica is like light clouds and showed an aggregate shape, while the as-synthesized $Fe_2O_3 \cdot SiO_2$ seems to become darker and denser after iron-loading, and $Fe_2O_3 \cdot SiO_2$ composite exhibited higher aggregation than silica due to impregnation and calcination processes, as can be seen in TEM images. Both samples were a bulk shape, which consisted of many small particles, approximately 10–20 nm in size. In TEM images, the iron oxide nanoparticles with about 5 nm in size were well dispersed on silica particles, while the iron oxide was not clearly distinguished from the silica in SEM images. The elemental composition of $Fe_2O_3 \cdot SiO_2$ composite from EDS stated that the composite contained 8.1 wt.% Fe and showed the dispersion of Fe on the surface of SiO_2 . The wide-angle XRD diffractions of SiO_2 and $Fe_2O_3 \cdot SiO_2$ composite showed that the diffraction peak of 20.1° belongs to amorphous silica, and the diffraction peaks at 21.8 , 25.0 , 35.39 , and 49.3° belong to α - Fe_2O_3 . The broad and low-intensity peaks of Fe_2O_3 could result from low loading deposition level, well dispersion, and poor crystalline structure with a small size of metal oxide particles in the composite. According to the N_2 adsorption/desorption isotherms of as-synthesized SiO_2 and as-synthesized $Fe_2O_3 \cdot SiO_2$ and IUPAC classification, both samples clearly showed a type II with an H1 hysteresis loop indicating material with agglomerates or compacts of approximately uniform spheres. The FT-IR spectra of the sample showed the small bands found at 685 and 604 cm^{-1} could be assigned to stretching vibrations of Fe-O and Si-O-Fe, respectively, which confirmed that SiO_2 indeed binds with Fe_2O_3 [17].

3.2.1.3 Clay-based catalysts

Clays such as montmorillonite, kaolin, and bentonite [18–20] are often employed as supporters in the use of heterogeneous catalysts, in order to lower the treatment cost of wastewater. Among the perspective clays, attapulgite clay is also a promising choice. Attapulgite clay is a kind of clay mineral with attapulgite as its main component. It is a crystalline hydrated magnesium aluminum silicate mineral with a unique layer-chain structure. Due to its particular structure, attapulgite has various excellent properties, such as good adsorption and catalytic properties [21–23]. Some examples of ATP for catalyst supporters are as below.

The first example is the preparation of the Fe_3O_4 /ATP catalyst [24]. ATP clay was mixed with water evenly and aged 24 h at room temperature. The aged ATP was granulated to microparticle and dried and then roasted. Spherical ATP particles were put into the mixture solution of thoroughly mixed oleylamine (or ethanol), and n-hexane was added with $Fe(acac)_3$ and immersed for a particular time in an ultrasonic instrument. After separating ATP particles from the mixture solution, they were dried at a vacuum drying oven and then the particles were put in a muffle furnace and roasted without air. Thus, the particle heterogeneous catalyst Fe_3O_4 /ATP was obtained. The process of preparing the Fe_3O_4 /ATP catalyst can be seen in **Figure 11**.

The characterizations of Fe_3O_4 /ATP are shown in **Figure 12**. Rod-shaped particles with lengths of 500~700 nm and widths of 100~150 nm are visible in SEM micrographs. After the introduction of iron species into ATP, nano- Fe_3O_4 particles were coated evenly onto the surface of ATP. TEM micrographs confirmed that the Fe_3O_4 nanoparticles with an average diameter of 10~25 nm stuck to the attapulgite rod-like fibers. The FT-IR results of Fe_3O_4 /ATP show some peaks at lower wave numbers (480 and 565 cm^{-1}) corresponding to vibration modes of Fe-O bonds of Fe_3O_4 nanoparticles on the surface of ATP. XRD patterns of Fe_3O_4 /ATP are contrasted with those of ATP. Sample Fe_3O_4 /ATP showed the characteristic peaks

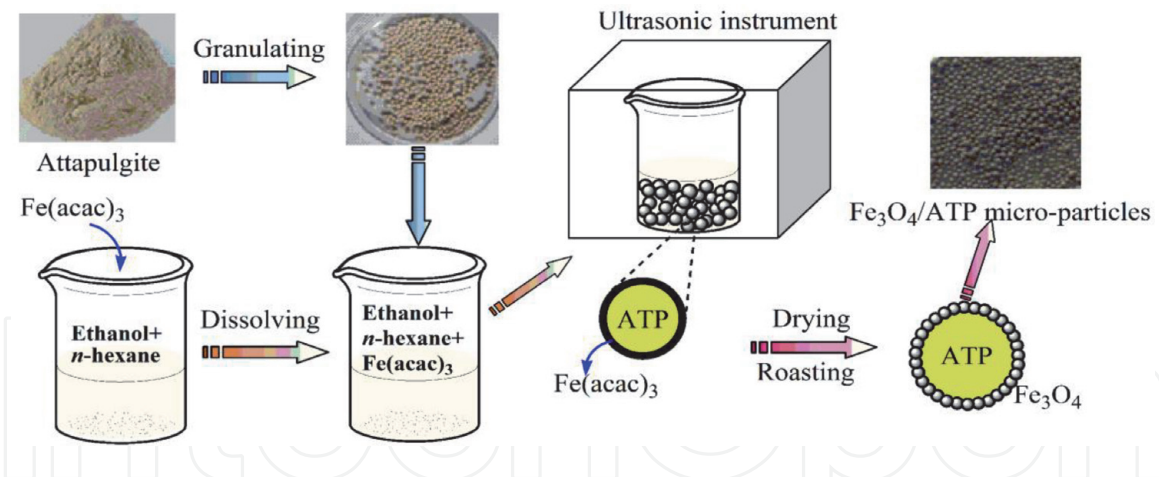


Figure 11. Schematic of preparing Fe₃O₄/ATP catalyst [24].

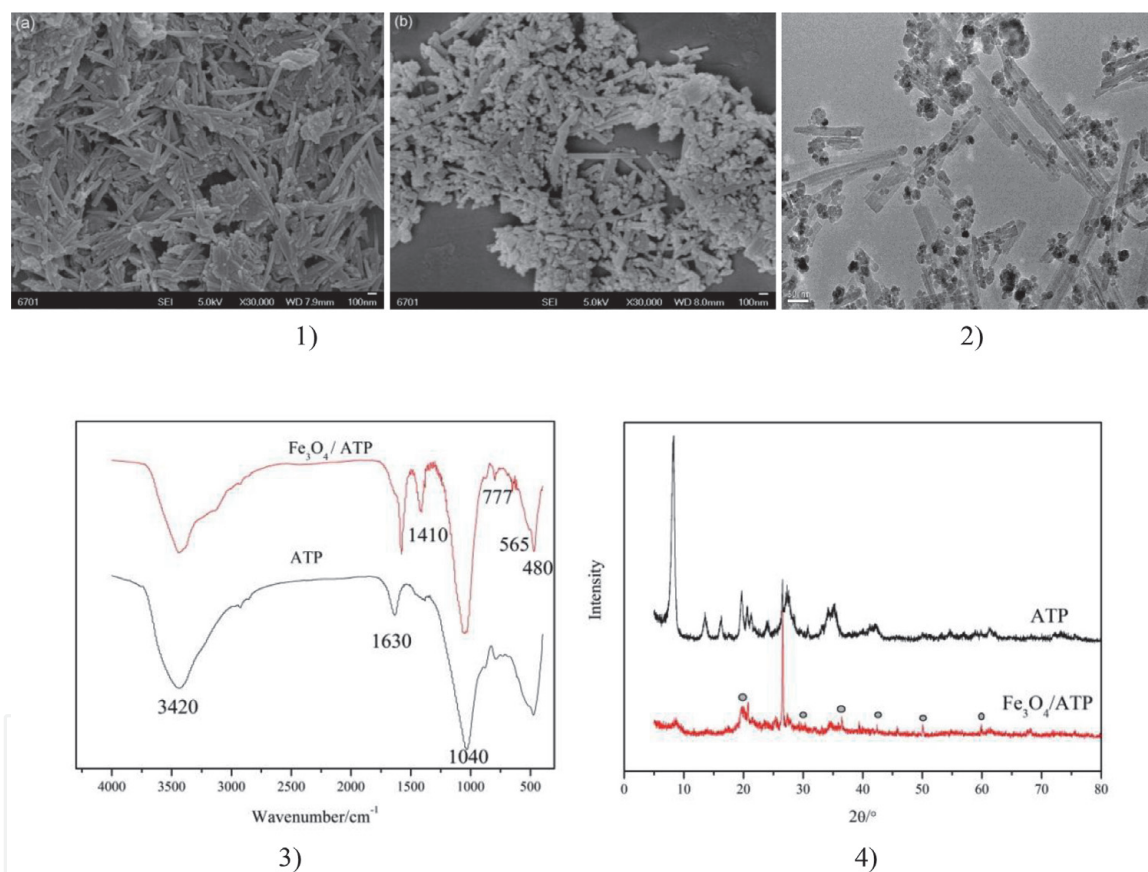


Figure 12. Characterizations of Fe₃O₄/ATP [24]. (1) SEM micrographs of samples (a) ATP, (b) Fe₃O₄/ATP. (2) TEM micrographs of Fe₃O₄/ATP. (3) FT-IR spectra of samples. (4) XRD patterns of samples.

(5.3, 8.4, 19.7, 27.5, 34.6, and 42.6°) of cubic spinel structure known from bulk Fe₃O₄ phase [24].

Some researchers organo-modified attapulgite to make it have a larger surface area and more pores. Fe/OATP is a kind of catalyst for HA-Na degradation, which employed organo-modified attapulgite as a supporter [25]. Attapulgite (ATP) was firstly acidified with 1 mol/L of HCl solution, then washed with distilled water three times, and dried. Octadecyl trimethyl ammonium chloride (OTAC) was weighed according to a particular proportion and dissolved in distilled water. Then acidified ATP was added into the OTAC solution at 60°C. The mixture was stirred and treated in an ultrasonic instrument for 15 minutes. After that, the clay was washed

with distilled water three times and dried in vacuum to obtain the organo-modified attapulgite (OATP). OATP and FeSO_4 were put into a beaker containing distilled water and stirred continuously. Sodium borohydride (NaBH_4) was slowly put into the beaker and stirred continuously. A large number of black floccules were produced. They were filtered and washed with ethanol for at least three times and dried in a vacuum drying oven to obtain the catalyst Fe/OATP. The synthesis process of Fe/OATP can be seen in **Figure 13**.

Characterizations of Fe/OATP are shown in **Figure 14** [25]. From SEM images, we can see that the length of the rod crystal had not changed after modification, but the layered structure, the surface area, and pore volume of the particles increase significantly, which means that the organic modification successfully enlarges the specific surface area of the ATP particles. After introducing nano-Fe into modified ATP particles (OATP), the spherical material with a diameter of about 80 nm is loaded on the rod structure of OATP, which showed that the nanoiron was loaded on the structure of OATP successfully. Some peaks, observed at 2923 and 2850 cm^{-1} in FT-IR curves of OATP and Fe/OATP samples, are symmetric stretching vibration peaks of $-\text{CH}_3$ and $-\text{CH}_2$, respectively. These peaks indicate that organics successfully modify attapulgite clay. After introducing the Fe species, the peaks at 2923 and 2850 cm^{-1} become weak. The strong peaks at 5.3 , 19.7 , 34.6 , 35.2 , 42.6 , and 78.7° could be found in the XRD patterns of all these three samples, which means the crystal structure of ATP has not been broken during the process of modification or preparation. The characteristic peaks at 50.4 , 61.9 , and 73.14° shown in the sample of Fe/OATP indicate that Fe^0 was successfully located on the clay structure [25].

3.2.2 Core-shell structured catalysts

In recent years, the preparation and application of core-shell structured materials have attracted extensive attention [26–28]. The catalysts compounded with the core-shell structure often exhibit high overall activity, large specific surface area, excellent shape-selective catalytic effect, and good thermal stability in catalytic reactions [29, 30]. The existence of shell layers not only provides available active

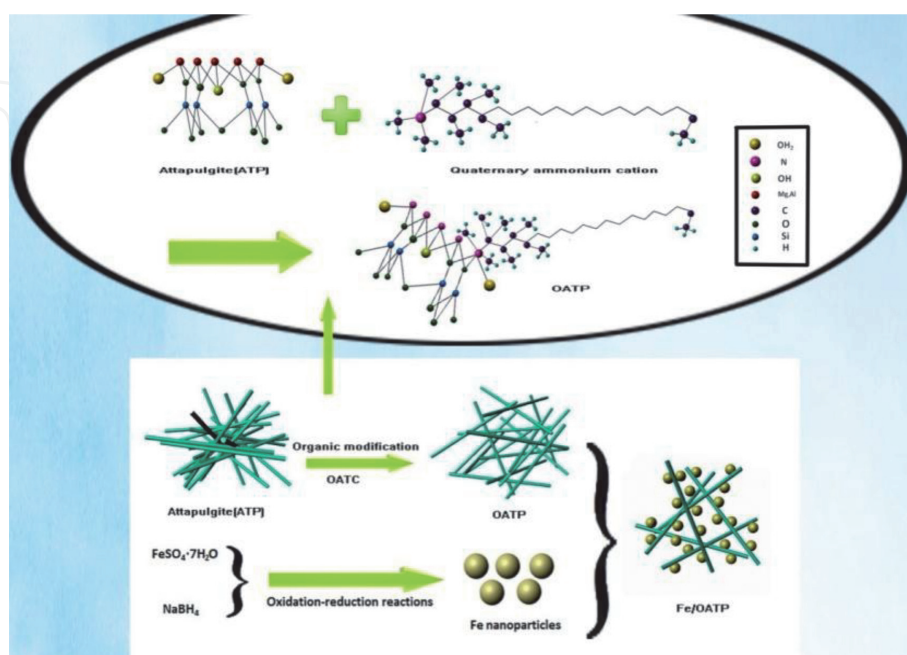


Figure 13.
Synthesis process of Fe/OATP [25].

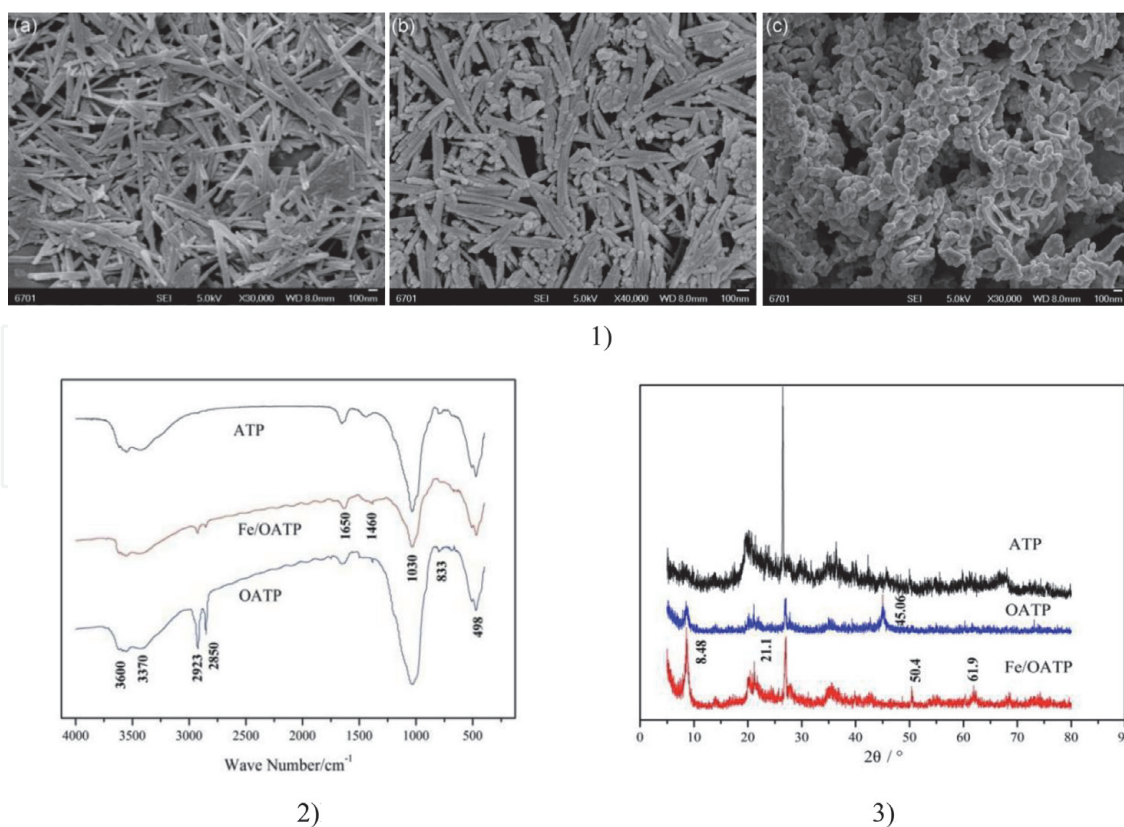


Figure 14.

Characterizations of Fe/OATP [25] (1) SEM images of the samples (a) ATP (b) OATP (c) Fe/OATP. (2) FT-IR spectroscopies of the samples (ATP, OATP, and Fe/OATP). (3) XRD patterns of the samples (ATP, OATP, and Fe/OATP).

sites for catalytic reactions but also protects for the core to avoid the collapse or sintering of the core catalyst structure leading to deactivation [31, 32].

Moreover, by selecting the chemical compositions of the core and shell, several inorganic substances with different characteristics can be incorporated into core-shell structure catalysts by appropriate methods, so that it can reach the goals of dual-function catalysis or even multifunction catalysis that single-component catalysts cannot achieve. It dramatically simplifies the experimental steps and saves precious time for researchers. Therefore, core-shell catalysts play an increasingly important role in the field of catalysis [33, 34]. The core-shell catalysts can comprise solid cores (such as inorganic, metal, or metal oxides) coated with polymers, inorganics, metal, or metal oxides [35–37]. The shell material can change the functionality, reactivity, and charge of the core surface, and also can strengthen the dispersibility and stability of the colloidal core. Catalytic or magnetic functions may be easily imparted to the colloidal core matter, depending on the coating materials. Metal oxides and zeolites are often used supporters of core-shell structured catalysts.

Ag@Fe₂O₃ core-shell structured catalysts were prepared using a homogeneous deposition precipitation method [38]. The core of silver colloids was first synthesized through a chemical reduction method using reagent grade silver nitrate as a precursor, NaBH₄, as the reducing agent and polyvinylpyrrolidone as the protecting agent. Then, an aqueous solution of urea and variable quantities of Fe₂(SO₄)₃·7H₂O were added to the solution of silver colloids. The mixture was heated for 1 h and then cooled to room temperature. The precipitate was washed thoroughly with warm water to remove as much sulfate ions as possible and then separated by centrifugation. At last, the product was dried. As shown in **Figure 15**, silver colloids

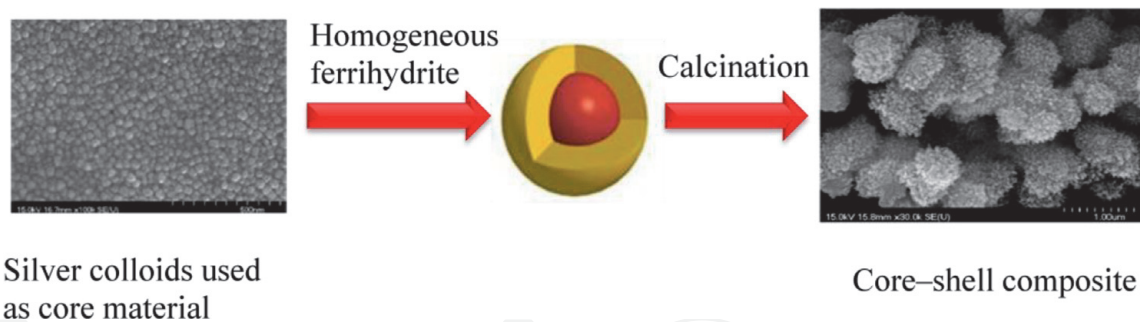


Figure 15.
Formation of $\text{Ag@Fe}_2\text{O}_3$ core-shell composite [38].

with about 40–50 nm in diameter were used as cores and the homogeneous ferrihydrite was used as shell. After being calcined, the rice-shaped $\text{Ag@Fe}_2\text{O}_3$ was formed, and the diameter and length of the $\text{Ag@Fe}_2\text{O}_3$ core-shell composite were about 10 and 20 nm, respectively. The calcined core-shell composites were aggregated with the size of 300–500 nm, which showed the porous nature of the $\text{Ag@Fe}_2\text{O}_3$ core-shell composite for catalytic reactions [38].

3.2.3 Thin-film catalysts

Thin films are a reliable and potential way of structuring the materials with tunable properties and flexible device construction in the field of energy and environment. It has gained technological importance as it helps to miniaturize the devices. Thin films are mostly modification methods to change the physical structure of materials. For example, the desired photocatalytic materials can be grown into thin films through the process of depositing molecular phase materials onto a substrate to form a solid material. The deposited thin films also can be grown along with the substrate and peeled off from the substrate and utilized as free-standing thin films. Thin-film catalysts have the potential to be used in the industries because synthesis processes of thin-film catalysts are simple in the handling of catalytic materials in several aspects such as their convenient design, adaptable form for the reactors, recyclability, recovery, etc. Therefore, the design of catalytic thin-film catalysts would be ideal for their wide applications.

Thin-film catalysts with good quality could be obtained by two methods: chemical depositions and physical depositions. Thin-film catalysts may consist of a layer and the substrate where the films are deposited on it, or consist of multiple layers. The following table shows different methods of thin-film deposition (**Table 2**) [40].

Thin-film catalysts can be used for hydrogen generation, photocatalytic CO_2 reduction to valuable chemicals, water treatment of toxic organic dyes, and bacterial disinfection. **Table 3** shows some examples of thin-film catalysts for water treatment.

For instance, Islam et al. have prepared zinc oxide (ZnO) and aluminum-doped zinc oxide (AZO) thin films onto a microscopic glass substrate using the sol-gel dip-coating technique at room temperature [49]. For both doped and undoped ZnO thin films, precursor solutions were prepared by dissolving $[\text{Zn}(\text{CH}_3\text{COO})_2 \cdot 2\text{H}_2\text{O}]$ in ethanol followed by stirring for 1 h; then, DEA was added as a stabilizer and water was added for hydrolysis. The resultant solution was stirred at room temperature for two more hours to obtain a clear and homogeneous sol. For AZO film, sols with different concentration of Al was prepared by dissolving an appropriate amount of $[\text{AlCl}_3 \cdot 6\text{H}_2\text{O}]$ and $[\text{Zn}(\text{CH}_3\text{COO})_2 \cdot 2\text{H}_2\text{O}]$ in ethanol. In both cases, the precursor solution was deposited on clean glass substrates by the dip-coating technique. The dip-coated thin films were dried at room temperature

Physical deposition	Evaporation techniques	Vacuum thermal evaporation
		Electron beam evaporation
		Laser beam evaporation
		Arc evaporation
	Sputtering techniques	Direct current sputtering
		Radiofrequency sputtering
Chemical deposition	Sol-gel technique	
	Chemical bath deposition	
	Spray pyrolysis technique	
	Plating	Electroplating technique
		Electroless deposition
	Chemical vapor deposition (CVD)	Low pressure chemical vapor deposition (LPCVD)
		Plasma-enhanced chemical vapor deposition (PECVD)
Atomic layer deposition (ALD)		

Table 2.
Different methods of thin-film deposition [39].

Thin films	Applications	Reference
TiO ₂ -anatase films	Trichloroethylene degradation	[41]
Au-buffered TiO ₂ thin films	Methylene blue degradation	[42, 43]
TiO ₂ /SiO _x	Dye degradation	[44]
ZnO thin films	Methylene blue degradation	
ZnO deposited on silicon	Dye degradation	[45]
ZnO nanorods grown on ZnO film	Dye degradation	[45]
α-Fe ₂ O ₃ thin films on Si(100) substrates	Dye degradation	[46]
SrTiO ₃ α-Fe ₂ O ₃ thin films	Dye degradation	[47]
PbO/TiO ₂	Stearic acid degradation	[48]

Table 3.
Different thin-film catalysts with application in wastewater treatment.

followed by calcinations at 400°C for 1 h to remove the organic compounds from the thin films.

Characterizations of Al-doped ZnO thin film can be seen in **Figure 16(a)** [49]. The crystal structure and different structural parameters of the films were analyzed from the X-ray diffraction (XRD) spectrum of the ZnO and AZO thin films. The undoped ZnO exhibits well-defined diffraction reflections corresponding to the wurtzite hexagonal phase of ZnO lattice planes. The intensity of all peaks decreases with Al doping suggesting deterioration of the crystallinity of ZnO films due to the incorporation of defects in the lattice site. From FE-SEM images, it can be seen that nanoparticles are formed and deposited on the film depositing area in all cases. For the pure ZnO thin film, the nanoparticle size varies from 10 to 70 nm. After the incorporation of Al, the particle size becomes more uniform, and the distribution of size is between 15 and 30 nm [49].

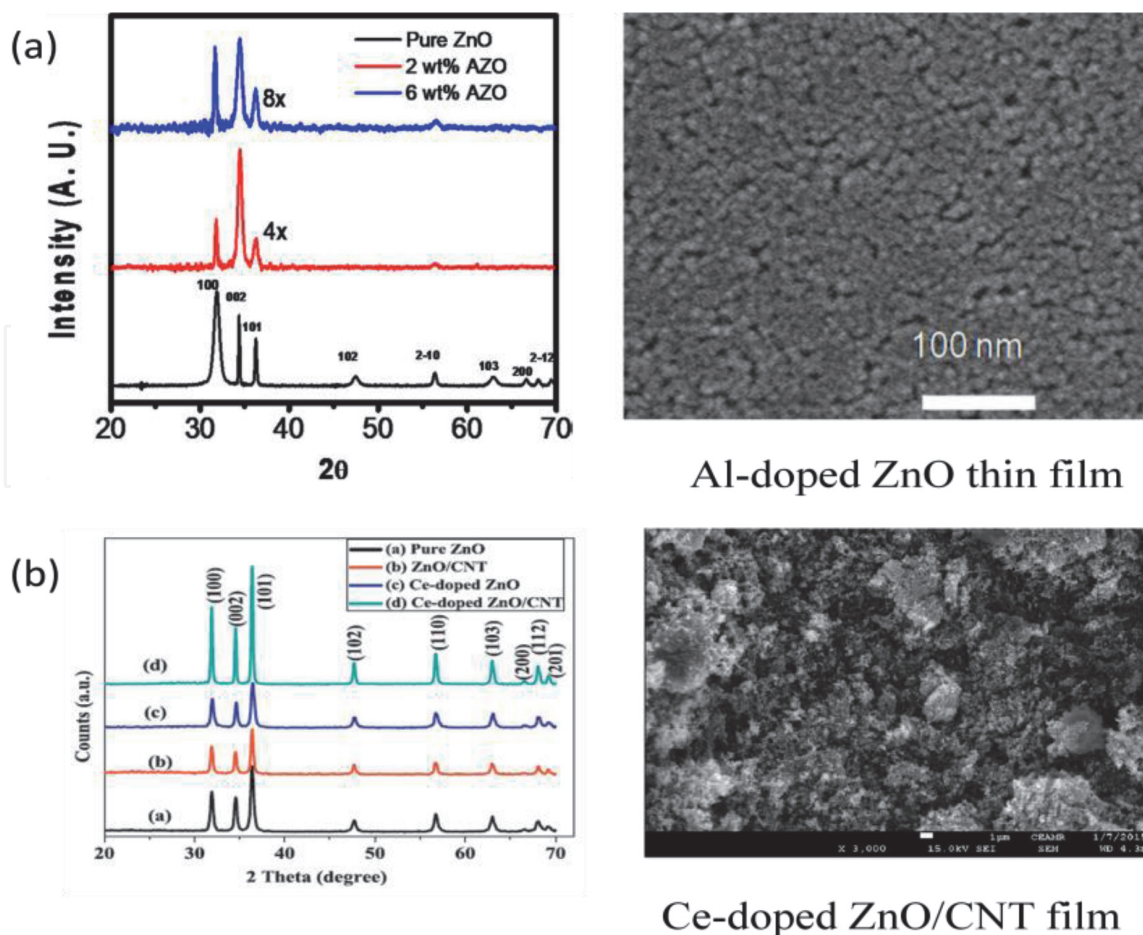


Figure 16. Characterizations of Al-doped ZnO thin film (a) and Ce-doped ZnO/CNT thin film (b) [49, 50].

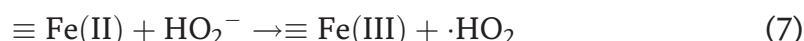
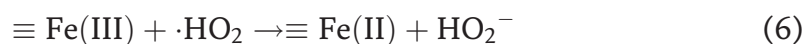
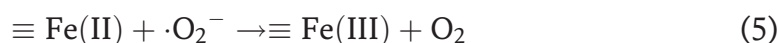
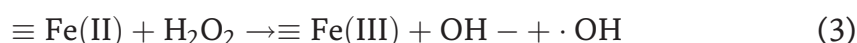
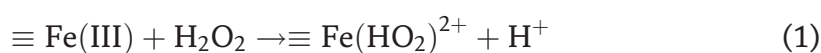
Another example is Ce-doped ZnO/carbon nanotube (CNT) thin film, which was prepared using a sol-gel drop coating method [50]. TEA and zinc acetate dehydrate were added into anhydrous ethanol under vigorous stirring. CNT and cerium sulfate were added into the above solution, and the solution was sonicated to get a uniform dispersion. The solution was heated at $(55 \pm 5)^\circ\text{C}$ with constant stirring at 200 rpm to get the ZnO/CNT sol, which was transparent and quite stable. The ZnO/CNT sol aged for 24 h before the preparation of the Ce-doped ZnO/CNT film. To synthesize Ce-doped ZnO/CNT thin film, the precursor solution was given dropwise on each of that frosted glass substrate using a pipette and then heated for 20 min at 80°C . The coating process was repeated twice for a thick film (~ 4 mm) preparation, and finally, the film was annealed at 500°C for 2 h using a muffle furnace.

To evaluate the crystallinity and crystal phases of the prepared thin film, XRD and FESEM spectra were acquired and are displayed in **Figure 16(b)** [50]. Ce and CeO_2 , Ce_2O_3 or other crystalline forms were not identified in the patterns, so the authors believed that Ce ions were uniformly substituted by Zn sites or interstitial sites in ZnO crystals. The addition of dopant and functionalized CNTs on the ZnO matrix presented the sharp and high-intense peak indicating the well-crystalline phase of ZnO. From the FESEM spectra of Ce-doped ZnO/CNT thin film, it is observed that that the sample ZnO/CNT is ZnO decorated on the surface of CNT, and the Ce-doped ZnO sample presents 3D flower-like microstructures consisting of many nanoflakes. It is worth noting that many different-size pores were generated in the 3D microstructures, which might act as transport paths for molecules and active sites for catalytic reaction and improve the catalytic properties of the thin-film material [50].

4. Heterogeneous catalysts for wastewater treatment: the process and mechanism

4.1 Heterogeneous Fenton catalysis

Heterogeneous Fenton catalysis, as one of the advanced oxidation technologies, is of great interest for environmental remediation owing to its benign process and general applicability [51]. Heterogeneous Fenton-like reactions on solid catalysts can effectively catalyze the oxidation of organic pollutants at wide pH conditions, which is beneficial for in situ remediations of polluted groundwater and soil and can be reused for further runs. Heterogeneous Fenton-like reaction is a surface-controlled reaction that depends on the catalyst surface area, on H_2O_2 concentration, on the reaction temperature, and on solution pH and ionic strength [52]. Kwan and Voelker [53] have suggested the chain of reactions in the catalyzed oxidation system as follows:



If only Fe(III) is originally present, Fe(II) is slowly generated by reactions (1) and (2) initiating oxidation reactions. A simple schematic of heterogeneous Fenton catalysis processes can be seen in **Figure 17**.

The magnetic $\text{Fe}_3\text{O}_4@ \beta\text{-CD/MWCNT}$ nanocomposites were prepared by a hydrothermal method and used as a heterogeneous Fenton-like catalyst to degrade Tetrabromobisphenol A (TBBPA) [54]. $\text{Fe}_3\text{O}_4@ \beta\text{-CD/MWCNT}$ presented good catalytic performance when removing TBBPA from water and got about 97% removal rate of under the optimum condition. Comodification of MWCNT and

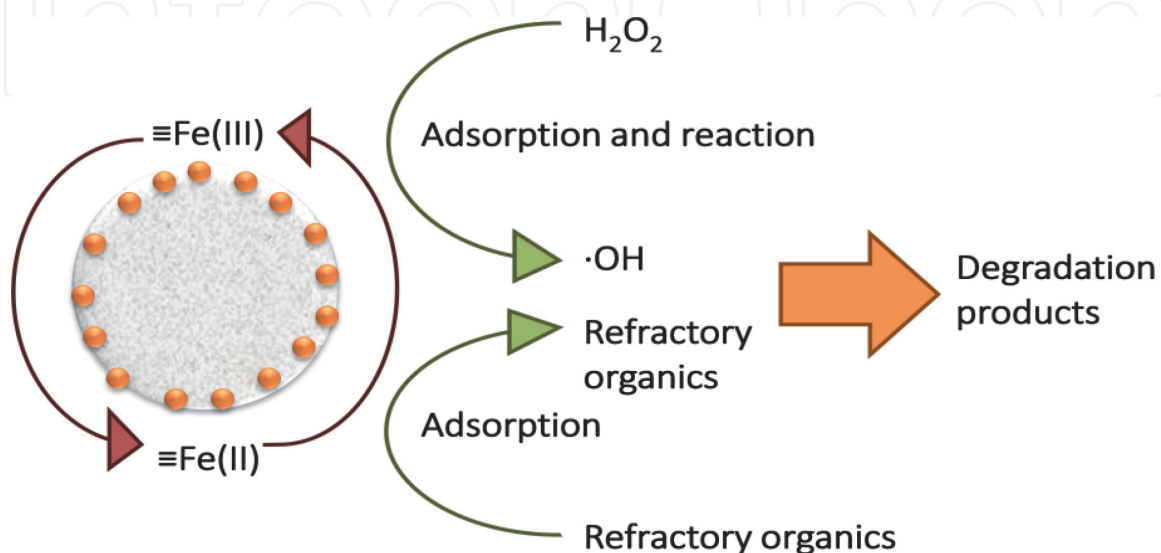


Figure 17.
A simple schematic of heterogeneous Fenton catalysis processes.

β -CD could distinctly promote the removal efficiency of TBBPA, which certified the existence of the synergistic effect between Fe_3O_4 , β -CD, and MWCNT. The catalyst has good regeneration ability; it still possessed excellent catalytic activity of TBBPA removal rate at about 86.2% after three cycles. Debromination and bridge fracture between two benzene rings were the primary process of TBBPA mineralization. This catalyst can provide a potential application in the degradation of refractory pollutants [54].

Except for Fe, Cu also can act as an active component of heterogeneous Fenton catalysts. Cu-V bimetallic catalyst (CuVO_x) with abundant surface defects was successfully synthesized by the hydrothermal method [55]. Degradation experiment of emerging pollutant fluconazole confirmed that CuVO_x exhibited higher catalytic activity, broader pH applicability, and more satisfactory reusability than monometallic copper compounds. By the introduction of vanadium into copper-based materials, several surface properties that are closely related to the reactivity of the copper catalysts, such as adsorption capacity, surface defects, and active site concentration, were improved. The electron-rich center around Cu/V active sites and surface oxygen vacancies are responsible for the rapid dissociation of H_2O_2 and the efficient catalytic oxidation of fluconazole in CuVO_x Fenton system. The introduction of vanadium increased active sites and electron density and improved the surface chemical properties of the bimetallic catalyst. FLC and H_2O_2 were firstly adsorbed on the surface of CuVO_x , which was beneficial to shorten the mass transfer process of pollutant oxidation. Around oxygen vacancies, there are abundant electrons with high transfer capability, which weaken the O-O bond of adsorbed H_2O_2 and transfer from the material surface to H_2O_2 . Under the reaction of catalyst, the adsorbed H_2O_2 was rapidly dissociated to produce a considerable amount of $\cdot\text{OH}$. Then, $\cdot\text{OH}$ attacked FLC adjacent to the active site, thereby achieving oxidative degradation of the pollutant [55].

4.2 Heterogeneous photocatalysis

Photocatalysis is the process of light-induced redox reactions upon the surrounding molecules to produce radical species for the subsequent utilization in

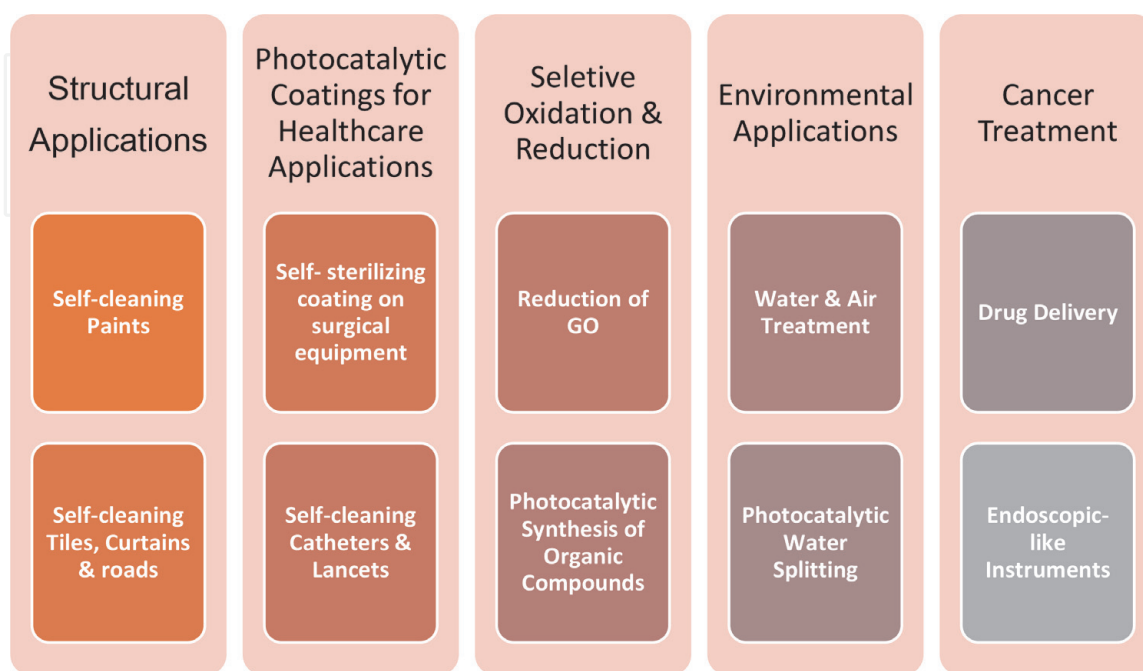


Figure 18.
Applications of heterogeneous photocatalysis [57].

various pollutant degradations, CO₂ conversion into hydrocarbon fuels, and disinfection of microorganisms, and so on, [56] as shown in **Figure 18**. Photocatalysis has many advantages: low reaction temperature, high oxidizability, complete purification, and using solar as an energy source. Furthermore, the careful selection of materials and structures of photocatalysts for photocatalysis is essential to perform the photocatalytic reactions efficiently. An ideal photocatalyst is bound to possess good performances such as narrow band gap energy, suitable band edge potential, reduced recombination, enhanced charge separation, and improved charge transportations [58]. For this purpose, photocatalytic materials are modified for their chemical compositions, which can be done through doping [59], composite formation [60], metal sensitization, and molecule functionalizations [61], among others, and physical structures, which include the size, shape, and surface morphology modifications of the materials.

The principle of photocatalysis is based on the theory of a solid energy band. When the energy of light irradiation absorbed by the semiconductor catalyst is larger than the photon band gap width, the electron-hole pairs are generated due to the transition of electrons. The light irradiation on the semiconductor causes the excitation of electrons from the valence band (VB) to the conduction band (CB) and the creation of holes in the valence band (VB) [62]. Electrons and holes stimulated by light radiation will migrate to the surface of semiconductor particles after various interactions and react with water or organics adsorbed on the surface of semiconductor catalyst particles to produce a photocatalytic effect, as shown in **Figure 19**. The typical photocatalytic process toward pollutant degradation can be described as follows.



Here are some examples of photocatalysis and photocatalysts.

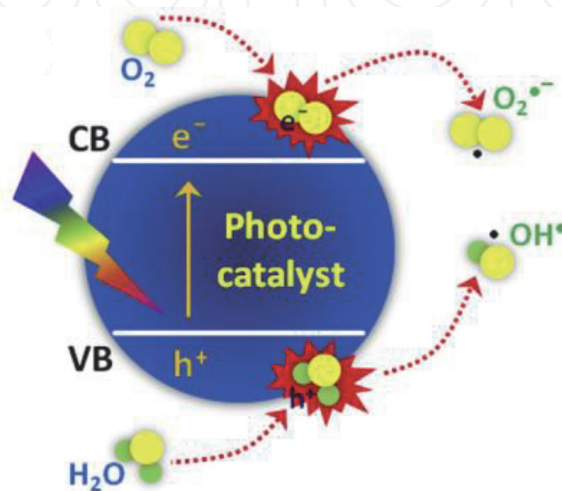


Figure 19.
Photocatalytic process in semiconductor.

A series of TiO₂/biochar composite catalysts were prepared by the hydrolysis method for the degradation of methyl orange, where biochar was obtained from the pyrolysis of waste walnut shells [63]. The photocatalytic activity results showed that TiO₂/biochar composite catalysts exhibited higher catalytic activity than that of pure TiO₂. The decolorization efficiency of 96.88% and the mineralization efficiency of 83.23% were obtained, attributed to the synergistic effect of biochar and TiO₂. After repeated uses, the catalyst still exhibited rather high activity toward the degradation of MO, where the decolorization efficiency and mineralization efficiency of MO achieved 92.45 and 76.56%, and the loss of activity was negligible. The possible degradation mechanism of MO with TiO₂/biochar composites can be explained as follows. MO molecules firstly adsorbed by biochar due to the well-developed pore structure, which provides more opportunities for the contact of catalysts and pollutants. With irradiation of ultraviolet light, TiO₂ was excited to generate electrons from the valence band, transferring to the conduction band, and holes were left in the valence band. Biochar transferred electrons and acted as acceptors, inhibiting the recombination of electron-hole pairs. Then, the electrons would react with oxygen molecules and water molecules to generate superoxide anion radicals and hydroxyl radicals. Holes would also be trapped by water molecules to engender hydroxyl radicals. Thus, holes, superoxide anion radicals, and hydroxyl radicals cofunctioned as active species would interact with the MO molecules, and finally, carbon dioxide was formed [63].

Sun et al. evaluated the photocatalytic efficiency of activated carbon-supported TiO₂ catalyst (AC/TiO₂) for degradation of aflatoxin B1 (AFB1) under UV-Vis light. AC/TiO₂ was prepared by simple hydrothermal synthesis [64]. According to the experiments, the higher degradation efficiency of AFB1 by AC/TiO₂ composite (98%) than that by bare TiO₂ (76%) was attributed to a higher surface area of AC/TiO₂ and enhanced visible-light intensity by the synergistic effect of TiO₂ and AC. Moreover, the catalyst can be easily separated from the solution and can still keep high activity. The authors found that the hole (h⁺) and the hydroxyl radicals (·OH) played an essential role in the degradation of AFB1 and proposed the possible photocatalytic oxidation mechanism of AC/TiO₂ for AFB1 degradation. When irradiated by UV light, the excited AC/TiO₂ composite produces electrons (e⁻) to the conduction band and holes (h⁺) on the valence band. The photo-generated electrons can react with O₂ to produce superoxide radicals (O₂^{-·}) and further produce hydroxyl radicals (·OH). The photo-generated holes can react with hydroxide ions (OH⁻) in the solution to directly produce ·OH. Some of these holes (h⁺) and ·OH would oxidize AFB1, which is absorbed on the surface of the catalyst [64]. Most of the photocatalysis processes have the same mechanism and they can be illustrated by (Figure 20).

4.3 Heterogeneous electrocatalysis

Electrocatalysis is a kind of catalysis that accelerates the charge transfer reaction at the interface of electrodes and electrolytes. The range of electrode catalysts is limited to electrical materials such as metals and semiconductors. There are many kinds of semiconductor oxides, such as skeleton nickel, nickel boride, tungsten carbide, sodium tungsten bronze, spinel and tungsten minerals, as well as various metals and phthalocyanines. Electrocatalysis is mainly used in the treatment of organic wastewater, degradation of chromium-containing wastewater, desulfurization of flue gas and raw coal, the simultaneous removal of NO_x and SO₂, and the reduction of carbon dioxide and nitrogen. The selection of appropriate electrode materials plays a critical role in accelerating the electrode reaction. The selected electrode materials play a catalytic role in the process of electrification, thus

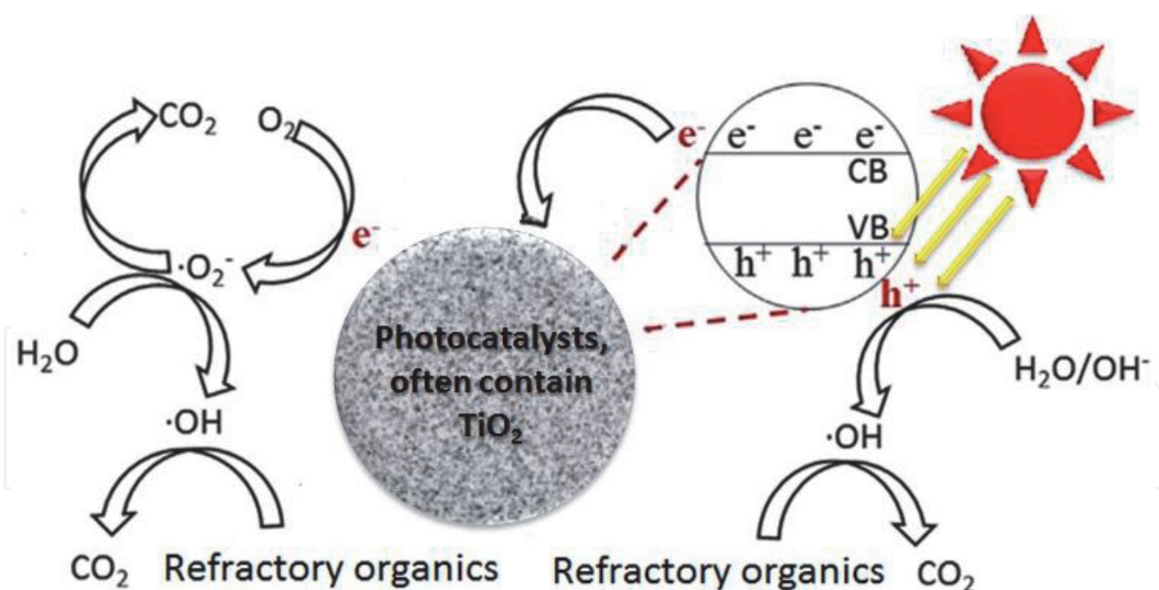


Figure 20.
The schematic of photocatalysis processes.

changing the reaction rate or direction of the electrode without any qualitative change in itself. Electrocatalysis covers two aspects of electrode reaction and catalysis, so electrocatalysts must have two functions at the same time: conductive and relatively free transfer of electrons; and effective catalytic activation. Therefore, the feasible way to design electrocatalysts is to modify the electrodes. Combining active components with conductive base electrodes in the form of covalent bonds or chemical adsorption can achieve the dual purposes of both transferring electrons and activating substrates.

Chao Zhang et al. investigated modified iron-carbon with polytetrafluoroethylene (PTFE) as a heterogeneous electro-Fenton (EF) catalyst for 2,4-dichlorophenol (2,4-DCP) degradation in near-neutral pH condition [65]. The degradation performance of the catalyst modification with 20% PTFE maintained well with low iron leaching. Moreover, the degradation efficiency of 2,4-DCP could exceed 95% within 120 min treatment at catalyst dosage of 6 g/L, initial pH of 6.7, and the current intensity of 100 mA. Two-stages of 2, 4-DCP degradation were observed: the first stage is a slow anodic oxidation stage, and the second one is a much faster heterogeneous EF oxidation stage. The automatic decrease of pH in the first stage initiated the Fe^{2+} release from microelectrolysis and benefited to the subsequent EF reaction. Aromatic intermediates including 2-chlorohydroquinone, 4,6-dichlororesorcinol, and 3,5-dichlorocatechol were detected by GC-MS. A possible mechanism and degradation pathway for 2,4-DCP were proposed. Air permeated from the prepared ADE cathode and was utilized to produce H_2O_2 . Simultaneously, Fe-C microelectrolysis would produce Fe^{2+} , which reacted with H_2O_2 as Fenton reagent. Considering the results of GC-MS and IC analyses, 2,4-DCP can be hydroxylated by $\cdot\text{OH}$ addition's reaction onto the aromatic ring, resulting in the formation of 3,5-dichlorocatechol and 4,6-dichlororesorcinol. Meanwhile, the chlorine atom located in the paraposition on the aromatic ring was substituted by $\cdot\text{OH}$ to yield 2-chlorohydroquinone. The aromatic organics mentioned above would be further oxidized to organic acids by $\cdot\text{OH}$, such as oxalic, acetic, and formic acids until mineralized to CO_2 completely. The possible degradation paths of 2,4-DCP can be seen in **Figure 21**.

Nanolayered double hydroxide (NLDH) decorated with Fe and Cu was applied as a novel heterogeneous catalyst for catalytic degradation of gentamicin by the electro-Fenton (EF) process [66]. The EF process was equipped with a graphite

plate under aeration. The highest removal efficiency was 91.3% when the Cu-Fe--NLDH-equipped EF process applied in comparison with the Fenton (50%) and the electro-oxidation alone (25.6%). Increasing the current resulted in the enhanced degradation of gentamicin, while the excessive electrolyte concentration and catalyst dosage led to the tangible drop in the reactor performance. At a specified reaction time, the injection of O₃ gas enhanced the efficiency of the Cu-Fe-NLDH-equipped EF process. The presence of ethanol led to a more suppressing effect than benzoquinone, indicating the dominant role of ·OH radical in the degradation of gentamicin compared with other free radical species such as O₂^{-·} radical. Most of

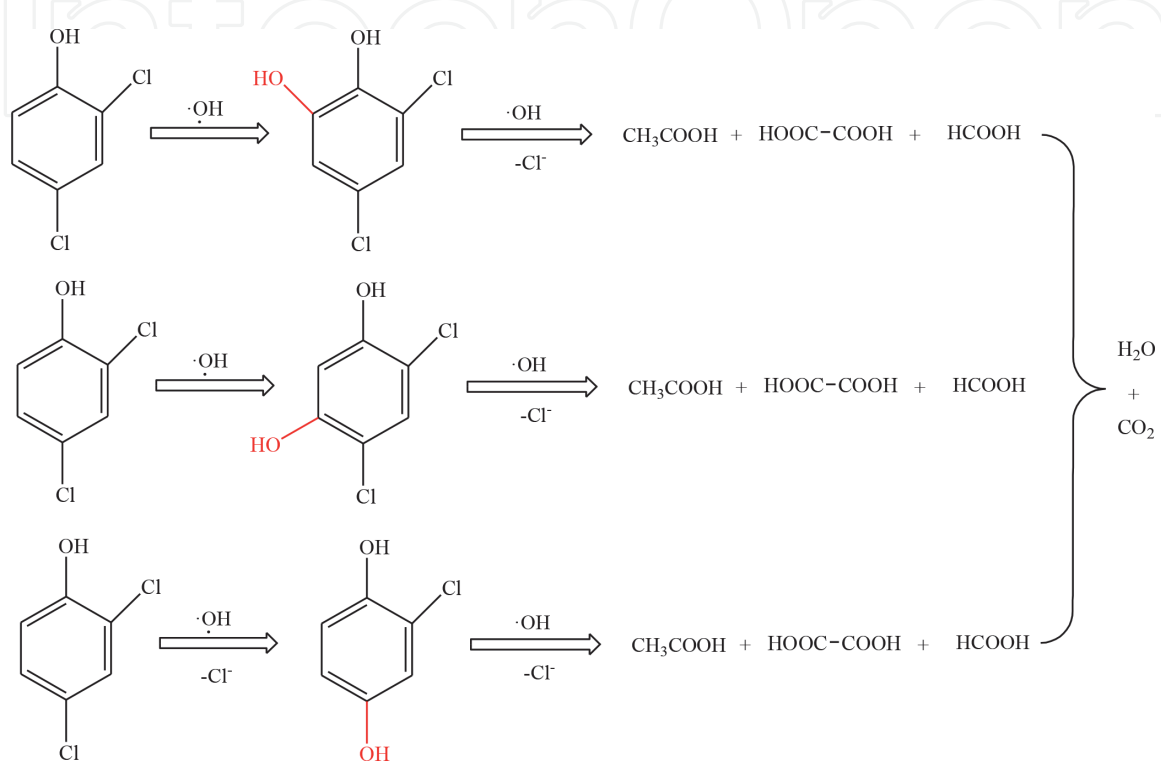


Figure 21.
 Proposed degradation pathway of 2,4-DCP [65].

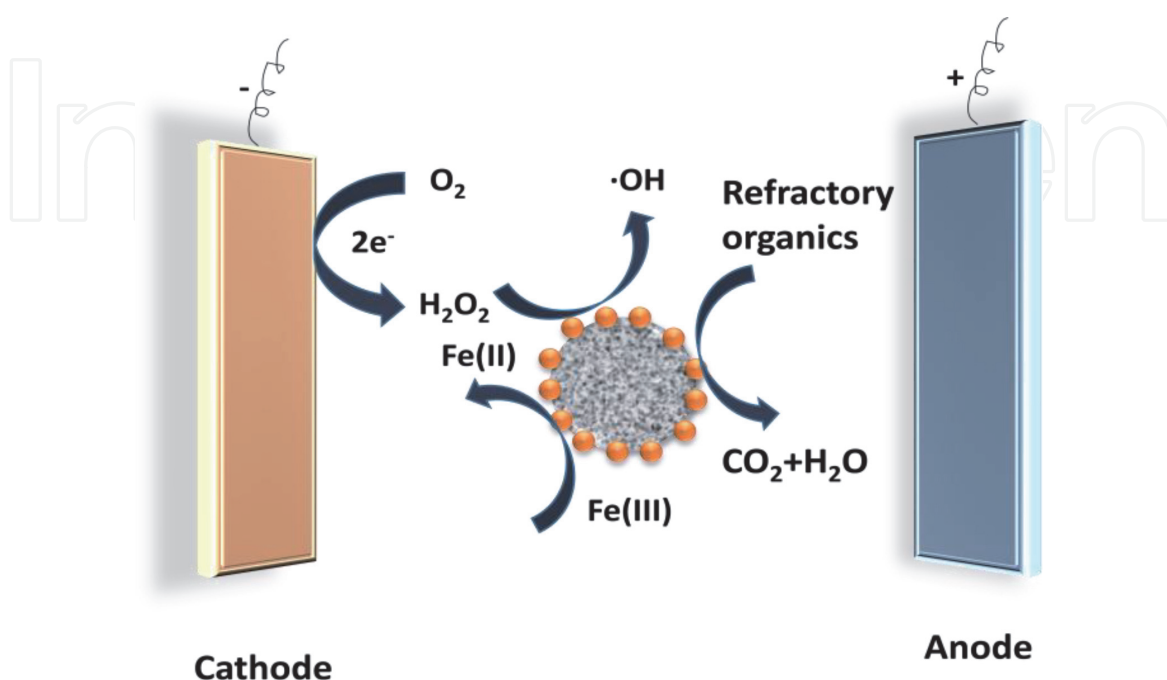


Figure 22.
 The schematic of electrocatalysis processes [66].

Catalysts	Target pollutants	Assistant	Degradation efficiency	Reference
Fe/OATP	HA-Na	—	97%	[24]
Fe ₃ O ₄ @β-CD/ MWCNT	Tetrabromobisphenol A	—	97%	[54]
CuVOx	Fluconazole	—	99%	[55]
Fe ₂ O ₃ /ATP	Methylene blue	—	99%	[67]
CuO/SiO ₂	RhB	—	95%	[68]
TiO ₂ /biochar	Methyl orange	UV-Vis light	98%	[63]
AC/TiO ₂	Aflatoxin B1	UV-Vis light	96.88%	[64]
Mg-ZnO-Al ₂ O ₃	Caffeine	UV-Vis light	98.9%	[69]
Fe-C/PTFE	2,4-DCP	Electric	95%	[65]
Cu-Fe-NLDH	Gentamicin	Electric	91.3%	[66]
DG@Fe ₃ O ₄	Methylene blue	Electric	99%	[70]

Table 4.
Comparison of some catalysts for different pollutant degradation.

the photocatalysis processes have the same mechanism, they just used different electrodes and catalysts, and they can be illustrated by (Figure 22).

The comparison of some catalysts for different pollutant degradation was shown in Table 4.

5. Conclusions

Heterogeneous catalytic processes, as an efficient green method coping with organic wastewater, have attracted considerable attention. Heterogeneous catalysts, such as bulk catalysts and supported catalysts (including surface-loaded catalysts, core-shell catalysts, and thin-film catalysts), are often synthesized by impregnation, sol-gel, and coprecipitation methods. To characterize heterogeneous catalysts, BET surface area, scanning electron microscope (SEM), transmission electron microscope (TEM), Fourier transform infrared spectroscopy (FT-IR), and X-ray diffraction (XRD) are common characterizing methods. Heterogeneous catalytic processes are efficient in treating organic wastewater due to the generation of highly reactive and nonselective hydroxyl radicals ($\cdot\text{OH}$), which can oxidize and mineralize most organic compounds, with the advantages of no secondary pollution, easy separation, and recycling. The researchers often employed heterogeneous catalysts to degrade dyes, pesticides, and antibiotics, among others. The reactions and mechanisms of different heterogeneous catalytic processes might be different according to the target pollutants.

At present, the researches on heterogeneous-supported catalysts should focus on the following problems: (1) how to prepare heterogeneous catalysts (especially nanocatalysts) with high efficiency, low cost, and low energy consumption, which can be widely used in the treatment of industrial wastewater; (2) how to prepare the catalysts with larger specific surface area and higher activity, and how to make the loaded active components distribute more evenly on the surface of the carrier; and (3) how to expand the application fields of heterogeneous catalysts, such as the application in degradation of microplastics in wastewater.

IntechOpen

IntechOpen

Author details

Ting Zhang
School of Petrochemical Engineering, Lanzhou University of Technology, Lanzhou,
China

*Address all correspondence to: zhangting@lut.cn

IntechOpen

© 2020 The Author(s). Licensee IntechOpen. Distributed under the terms of the Creative Commons Attribution - NonCommercial 4.0 License (<https://creativecommons.org/licenses/by-nc/4.0/>), which permits use, distribution and reproduction for non-commercial purposes, provided the original is properly cited. 

References

- [1] Taylor HS. Catalysis—Chemical Process. 1957. Available from: www.britannica.com
- [2] Wang Q, Tian S, Long J, Ning P. Use of Fe(II)Fe(III)-LDHs prepared by co-precipitation method in a heterogeneous-Fenton process for degradation of methylene blue. *Catalysis Today*. 2014;41-48
- [3] Cheng M, Ma W, Li J, Huang Y, Zhao J, Wen YX, et al. Visible-light-assisted degradation of dye pollutants over Fe(III)-loaded resin in the presence of H₂O₂ at neutral pH values. *Environmental Science & Technology*. 2004;38:1569-1575
- [4] Socci J, Osatiashtiani A, Kyriakou G, Bridgwater T. The catalytic cracking of sterically challenging plastic feedstocks over high acid density Al-SBA-15 catalysts. *Applied Catalysis A: General*. 2019;570:218-227
- [5] Lu P, Cai F, Zhang J, Liu Y, Sun Y. Hydrogen production from methanol steam reforming over B-modified CuZnAlO_x catalysts. *Journal of Fuel Chemistry and Technology*. 2019;47:791-798
- [6] Cai F, Lu P, Ibrahim JJ, Fu Y, Zhang J, Sun Y. Investigation of the role of Nb on Pd–Zr–Zn catalyst in methanol steam reforming for hydrogen production. *International Journal of Hydrogen Energy*. 2019;44:11717-11733
- [7] Islam M, Basnayake R, Korzeniewski C. A study of formaldehyde formation during methanol oxidation over PtRu bulk alloys and nanometer scale catalyst. *Journal of Electroanalytical Chemistry*. 2007;599:31-40
- [8] Ji F, Li C, Zhang J, Deng L. Heterogeneous photo-Fenton decolorization of methylene blue over LiFe(WO₄)₂ catalyst. *Journal of Hazardous Materials*. 2011;186:1979-1984
- [9] Duan F, Yang Y, Li Y, Cao H, Wang Y, Zhang Y. Heterogeneous Fenton-like degradation of 4-chlorophenol using iron/ordered mesoporous carbon catalyst. *Journal of Environmental Sciences*. 2014;26:1171-1179
- [10] Hu X, Liu B, Deng Y, Chen H, Luo S, Sun C, et al. Adsorption and heterogeneous Fenton degradation of 17 α -methyltestosterone on nano Fe₃O₄/MWCNTs in aqueous solution. *Applied Catalysis B: Environmental*. 2011;107:274-283
- [11] Molina R, Martínez F, Melero JA, Bremner DH, Chakinala AG. Mineralization of phenol by a heterogeneous ultrasound/Fe-SBA-15/H₂O₂ process: Multivariate study by factorial design of experiments. *Applied Catalysis B: Environmental*. 2006;66:198-207
- [12] Muthukumari B, Selvam K, Muthuvel I, Swaminathan M. Photoassisted hetero-Fenton mineralization of azo dyes by Fe(II)-Al₂O₃ catalyst. *Chemical Engineering Journal*. 2009;153:9-15
- [13] Vignesh K, Rajarajan M, Suganthi A. Visible light assisted photocatalytic performance of Ni and Th co-doped ZnO nanoparticles for the degradation of methylene blue dye. *Journal of Industrial and Engineering Chemistry*. 2014;20:3826-3833
- [14] Panda N, Sahoo H, Mohapatra S. Decolourization of methyl orange using Fentonlike mesoporous Fe₂O₃–SiO₂ composite. *Journal of Hazardous Materials*. 2011;185:359-365
- [15] Zhong X, Royer S, Zhang H, Huang Q, Xiang L, Valange S, et al.

- Mesoporous silica iron-doped as stable and efficient heterogeneous catalyst for the degradation of C.I. acid orange 7 using sono-photo-Fenton process. *Separation and Purification Technology*. 2011;**80**:163-171
- [16] Liu T, You H, Chen Q. Heterogeneous photo-Fenton degradation of polyacrylamide in aqueous solution over Fe(III)-SiO₂ catalyst. *Journal of Hazardous Materials*. 2009;**162**:860-865
- [17] Vu AT, Xuan TN, Lee CH. Preparation of mesoporous Fe₂O₃-SiO₂ composite from rice husk as an efficient heterogeneous Fenton-like catalyst for degradation of organic dyes. *Journal of Water Process Engineering*. 2019;**28**: 169-180
- [18] Chen JX, Zhu LZ. Catalytic degradation of Orange II by UV-Fenton with hydroxyl-Fe-pillared bentonite in water. *Chemosphere*. 2006;**65**: 1249-1225
- [19] Chen JX, Zhu LZ. Oxalate enhanced mechanism of hydroxyl-Fe-pillared bentonite during the degradation of Orange II by UV-Fenton process. *Journal of Hazardous Materials*. 2011; **185**:1477-1481
- [20] Feng JY, Hu XJ, Yue PL. Discoloration and mineralization of Orange II by using a bentonite clay-based Fe nanocomposite film as a heterogeneous photo-Fenton catalyst. *Water Research*. 2005;**39**:89-96
- [21] Perderiset M, Baillif P, Jaurand MC. Chemical analysis and photoelectron spectroscopy of the adsorption of macromolecules on the surface of attapulgite. *Journal of Colloid and Interface Science*. 1988;**121**:381-391
- [22] Zhang J, Chen H, Wang A. Study on superabsorbent composite. III. Swelling behaviors of polyacrylamide/attapulgite composite based on acidified attapulgite and organo-attapulgite. *European Polymer Journal*. 2005;**41**:2434-2442
- [23] Li A, Zhang JP, Wang AQ. Utilization of starch and clay for the preparation of superabsorbent composite. *Bioresource Technology*. 2007;**98**:327-332
- [24] Zhang T, Qian C, Dong L. Preparation of particle reusable heterogeneous catalyst Fe₃O₄/ATP for methylene blue decolorization. *International Journal of Environmental Science and Technology*. 2019;**10**: 343-349
- [25] Zhang T, Liu J, Chen M, Wang Y. Preparation of heterogeneous Fenton catalyst Fe/organ-attapulgite and its performance in sodium humate degradation. *Desalination and Water Treatment*. 2018;**107**:91-99
- [26] Solar P, Polonskyi O, Olbricht A, Hinz A, Shelemin A, Kylián O, et al. Single step generation of metal-plasma polymer multicore@shell nanoparticles from the gas phase. *Scientific Reports*. 2017;**7**: 8514-8519
- [27] Martinez L, Mayoral A, Espineira M, Roman E, Palomares FJ, Huttel Y. Core@ shell, Au@ TiO_x nanoparticles by gas phase synthesis. *Nanoscale*. 2017; **9**:6463-6470
- [28] Solaiyammal T, Murugakoothan P. Green synthesis of Au and Au@ TiO₂ core-shell structure formation by hydrothermal method for dye sensitized solar cell applications. *Journal of Materials Science: Materials in Electronics*. 2018;**29**:1-9
- [29] Guo XH, Ma JQ, Ge HG. CoFe₂O₄@ TiO₂@ Au core-shell structured microspheres: Synthesis and photocatalytic properties. *Russian Journal of Physical Chemistry A*. 2017; **91**:2643-2650

- [30] Shi BN, Wan JF, Liu CT, Yu XJ, Ma FW. Synthesis of $\text{CoFe}_2\text{O}_4/\text{MCM-41}/\text{TiO}_2$ composite microspheres and its performance in degradation of phenol. *Materials Science in Semiconductor Processing*. 2015;**37**:241-249
- [31] Sohail M, Xue H, Jiao Q, Li H, Khan K, Wang S, et al. Synthesis of well-dispersed $\text{TiO}_2/\text{CNTs}@ \text{CoFe}_2\text{O}_4$ nanocomposites and their photocatalytic properties. *Materials Research Bulletin*. 2018;**101**:83-89
- [32] Hang S, He Q, Ping S, Zeng S, Xu K, Li J, et al. One-pot synthesis of $\text{Au}@ \text{TiO}_2$ yolk-shell nanoparticles with enhanced photocatalytic activity under visible light. *Journal of Colloid and Interface Science*. 2017;**505**:884-891
- [33] Ma JQ, Guo SB, Guo XH, Ge HG. Liquid-phase deposition of TiO_2 nanoparticles on core-shell $\text{Fe}_3\text{O}_4 @ \text{SiO}_2$ spheres: Preparation, characterization, and photocatalytic activity. *Journal of Nanoparticle Research*. 2015;**17**:1-11
- [34] Wu J, Yang Y, Ding J. Green production of cyclohexanone oxime with a fixed-bed reactor using shaped titanosilicate catalysts. *Chinese Journal*. 2015;**60**:1538-1545
- [35] Caruso F. Nanoengineering of particle surfaces. *Advanced Materials*. 2010;**13**:11-19
- [36] Reiss P, Protiere M, Li L. Core/shell semiconductor nanocrystals. *Small*. 2009;**5**:154-168
- [37] Shi ZL, Du C, Yao SH. Preparation and photocatalytic activity of cerium doped anatase titanium dioxide coated magnetite composite. *Journal of the Taiwan Institute of Chemical Engineers*. 2011;**42**:652-657
- [38] Chou KS, Lin MY, Wu HH. Studies on the removal of 2-propanol by $\text{Ag}@ \text{Fe}_2\text{O}_3$ core-shell structured catalyst. *Journal of the Taiwan Institute of Chemical Engineers*. 2013;**44**:228-232
- [39] Jilani A, Abdel-Wahab MS, Hammad AH. *Advance Deposition Techniques for Thin Film and Coating*. London: IntechOpen; 2017
- [40] Shwetharani R, Chandan HR, Sakar M, Balakrishna GR, Reddy KR, Raghu AV. Photocatalytic semiconductor thin films for hydrogen production and environmental applications. *International Journal of Hydrogen Energy*. 2019. DOI: 10.1016/j.ijhydene.2019.03.149
- [41] Arconada N, Suarezb DAS, Portelab R, Coronadob JM, Sanchezb B, Castro Y. Synthesis and photocatalytic properties of dense and porous TiO_2 -anatase thin films prepared by sol-gel. *Applied Catalysis B: Environmental*. 2009;**86**:1-7
- [42] Sakthivel S, Shankar MV, Palanichamy M, Arabindoo B, Bahnemann DW, Murugesan V. Enhancement of photocatalytic activity by metal deposition: Characterization and photonic efficiency of Pt, Au, and Pd deposited on TiO_2 catalyst. *Water Research*. 2004;**38**:3001-3008
- [43] Jung JM, Wang M, Kim EJ, Park C, Hahn SH. Enhanced photocatalytic activity of Au-buffered TiO_2 thin films prepared by radio frequency magnetron sputtering. *Applied Catalysis B: Environmental*. 2008;**84**:389-392
- [44] Seong SG, Kim EJ, Kim YS, Lee KE, Hahn SH. Influence of deposition atmosphere on photocatalytic activity of $\text{TiO}_2/\text{SiO}_x$ double-layers prepared by RF magnetron sputtering. *Applied Surface Science*. 2009;**256**:1-5
- [45] Di Mauro A, Fragala ME, Privitera V, Impellizzeri G. ZnO for application in photocatalysis: From thin films to nanostructures. *Materials*

Science in Semiconductor Processing. 2017;**69**:44-51

[46] Chen YH, Tu KJ. Thickness dependent o photocatalytic activity of hematite thin films. *International Journal of Photoenergy*. 2012; **1110-662X**:1-6

[47] Schultz AM, Salvador PA, Rohrer GS. Enhanced photochemical activity of α -Fe₂O₃ films supported on SrTiO₃ substrates under visible light illumination. *Chemical Communications*. 2012;**48**:2012-2014

[48] Bhachu DS, Sathasivam S, Carmalt CJ, Parkin IP. PbO modified TiO₂ thin films: A route to visible light photocatalysts. *Langmuir*. 2014;**30**: 624-630

[49] Islam MR, Rahman M, Farhad SFU, Podder J. Structural, optical and photocatalysis properties of sol-gel deposited Aldoped ZnO thin films. *Surface and Interface Analysis*. 2019;**16**: 120-126

[50] Elias M, Uddin MN, Hossain MA, Saha JK, Siddiquey IA, Sarker DR, et al. An experimental and theoretical study of the effect of Ce doping in ZnO/CNT composite thin film with enhanced visible light photo-catalysis. *International Journal of Hydrogen Energy*. 2019;**44**:20068-20078

[51] Xia M, Chen C, Long M, Chen C, Cai W, Zhou B. Magnetically separable mesoporous silica nanocomposite and its application in Fenton catalysis. *Microporous and Mesoporous Materials*. 2011;**145**:217-223

[52] Matta R, Hanna K, Chiron S. Fenton-like oxidation of 2,4,6-trinitrotoluene using different iron minerals. *Science of the Total Environment*. 2007;**385**:242-251

[53] Kwan WP, Voelker BM. Rates of hydroxyl radical generation and organic

compound oxidation in mineral-catalyzed Fenton-like systems. *Environmental Science & Technology*. 2005;**39**:9303-9308

[54] Zhang Y, Wu P, Chen Z, Zhou L, Zhao Y, Lai Y, et al. Synergistic effect in heterogeneous Fenton degradation of tetrabromobisphenol a by MWCNT and β -CD co-modified Fe₃O₄. *Materials Research Bulletin*. 2019;**113**:14-24

[55] Zhang N, Xue C, Wang K, Fang Z. Efficient oxidative degradation of fluconazole by a heterogeneous Fenton process with Cu-V bimetallic catalysts. *Chemical Engineering Journal*. 2020; **380**:122516

[56] Francis O, Kuben GK, Sittert CGCE, Poomani GP. Recent progress in the development of semiconductor-based photocatalyst materials for applications in photocatalytic water splitting and degradation of pollutants. *Advanced Sustainable Systems*. 2017: 1700006

[57] Ahmed SN, Haider W. Heterogeneous photocatalysis and its potential applications in water and wastewater treatment: A review. *Nanotechnology*. 2018;**29**: 342001

[58] Reddy KR, Reddy CV, Nadagouda MN, Shetti NP, Jaesool S, Aminabhavi TM. Polymeric graphitic carbon nitride (g-C₃N₄)-based semiconducting nanostructured materials: Synthesis methods, properties and photocatalytic applications. *Journal of Environmental Management*. 2019; **238**:25-40

[59] Ravikumar CH, Mahto MSA, Nanjundaiah RT, Thippeswamy R, Teixeira SR, Balakrishna RG. Observation of oxo-bridged yttrium in TiO₂ nanostructures and their enhanced photocatalytic hydrogen generation under UV/visible light irradiations.

- Materials Research Bulletin. 2018;**104**: 212-219
- [60] D'Souza LP, Muralikrishna S, Chandan HR, Ramakrishnappa T, Balakrishna RG. Neodymium doped titania as photoanode and graphene oxide-CuS composite as a counter electrode material in quantum dot solar cell. *Journal of Materials Research*. 2015; **30**:3241-3251
- [61] Schiffman HRCJD, Balakrishna RG. Quantum dots as fluorescent probes: Synthesis, surface chemistry, energy transfer mechanisms, and applications. *Sensors and Actuators B: Chemical*. 2018;**258**:1191-1214
- [62] Ibhaddon A, Fitzpatrick P. Heterogeneous photocatalysis: Recent advances and applications. *Catalysts*. 2013;**3**:189
- [63] Lu L, Shan R, Shi Y, Wang S, Yuan H. A novel TiO₂/biochar composite catalysts for photocatalytic degradation of methyl orange. *Chemosphere*. 2019;**222**:391-398
- [64] Sun S, Zhao R, Xie Y, Liu Y. Photocatalytic degradation of aflatoxin B1 by activated carbon supported TiO₂ catalyst. *Food Control*. 2019;**100**: 183-188
- [65] Zhang C, Zhou M, Ren G, Yu X, Ma L, Yang J, et al. Heterogeneous electro-Fenton using modified iron-carbon as catalyst for 2,4-dichlorophenol degradation: Influence factors, mechanism and degradation pathway. *Water Research*. 2015;**70**: 414-424
- [66] Ghasemi M, Khataee A, Gholami P, Soltani RDC. Template-free microspheres decorated with Cu-Fe-NLDH for catalytic removal of gentamicin in heterogeneous electro-Fenton process. *Journal of Environmental Management*. 2019;**248**: 109236
- [67] Zhang T, Chen M, Yu S. Decolorization of methylene blue by an attapulgite-based heterogeneous Fenton catalyst: Process optimisation. *Desalination and Water Treatment*. 2017;**63**:275-282
- [68] Sun Y, Tian P, Ding D, Yang Z, Wang W, Xin H, et al. Revealing the active species of Cu-based catalysts for heterogeneous Fenton reaction. *Applied Catalysis B: Environmental*. 2019;**258**: 117985
- [69] Elhalil A, Elmoubarki R, Farnane M, Machrouhi A, Sadiq M, Mahjoubi FZ, et al. Photocatalytic degradation of caffeine as a model pharmaceutical pollutant on Mg doped ZnO-Al₂O₃ heterostructure. *Environmental Nanotechnology, Monitoring and Management*. 2018;**10**:63-72
- [70] Wang J, Yang F, Wang S, Zhong H, Wu Z, Cao Z. Reactivation of nano-Fe₃O₄/diethanolamine/rGO catalyst by using electric field in Fenton reaction. *Journal of the Taiwan Institute of Chemical Engineers*. 2019;**99**:113-122